Afdelingen for Bærende Konstruktioner
Department of Structural Engineering
Danmarks Tekniske Højskole · Technical University of Denmark

PRELIMINARY STATE-OF-THE-ART REPORT ON MULTIAXIAL STRENGTH OF CONCRETE

KAARE K. B. DAHL

Serie R No 262 1990

PRELIMINARY
STATE-OF-THE-ART REPORT
ON
MULTIAXIAL STRENGTH OF CONCRETE

KAARE K. B. DAHL

Preliminary State-of-the-art Report on Multiaxial Strength of Concrete

Tryk:
Afdelingen for Bærende Konstruktioner
Danmarks Tekniske Højskole
Lyngby
ISBN 87-7740-040-2

SUMMARY

This report deals with the strength of concrete subjected to triaxial stress fields.

The report describes some of the more important failure criteria for concrete. Furthermore a description of the possible factors that affects, or is thought to affect, the triaxial strength of concrete is included. Also in the report is a description of the various test arrangements used through the years. These test arrangements all have strengths and weaknesses which are described. Finally most of the published strength results are presented, along with a bibliography over the published research.

LIST OF CONTENTS

NOTATION

A_i	Internal area per unit concrete area, $A_i \leq 1$.
A	Parameter in the Ottosen failure criterion.
B	Parameter in the Ottosen failure criterion.
D	Smallest dimension of a casting form.
K_1	Parameter in the Ottosen failure criterion.
K_2	Parameter in the Ottosen failure criterion.
I_1, I_2, I_3	Invariants of the stress tensor.
J_1, J_2, J_3	Invariants of the deviatoric stress tensor.
V_{aggr}	Aggregate volume content $V_{aggr} \leq 1$.
d	Maximum aggregate size.
f_c	Uniaxial compressive strength of concrete.
f_{cc}	Equal biaxial compressive strength of concrete.
f'_{cc}	Equal biaxial compressive strength normalized with the uniaxial compressive strength.
f_t	Uniaxial tensile strength of concrete.
f'_t	Uniaxial tensile strength normalized with the uniaxial compressive strength.
k	Coefficient in the Mohr–Coulomb criterion $k = f_c/f_t$.
k_1, k_2	Factor.
n_1, n_2, n_3	Principal axes.
s_{ij}	Deviatoric stress field.
s_1, s_2, s_3	Principal deviatoric stresses.
α	Parameter in the Willam – Warnke failure criterion.
δ_{ij}	Kroneckers delta.
θ	Angle in the deviatoric plane.
λ	Function that describes the deviatoric plane, Ottosen failure criterion.
ρ	Length of a vector in the deviatoric plane.
ρ_c	Parameter in the Willam – Warnke failure criterion.
ρ_t	Parameter in the Willam – Warnke failure criterion.
σ	Normal stress.
$\sigma_1, \sigma_2, \sigma_3$	Principal stresses.

σ_{ij}	Stress tensor.
$\sigma_{i,true}$	Resulting principal stress.
σ_m	Mean normal stress.
σ_{oct}	Octahedral normal stress.
σ_{pore}	Pore pressure.
τ	Shear stress.
τ_m	Mean shear stress.
τ_{oct}	Octahedral shear stress.
ξ	Length of a vector along the hydrostatic axis.
ψ	Angle.

Chapter 1

INTRODUCTION

Advances in the design of concrete structures are placing an ever increasing emphasis on the need for knowledge concerning the strength of concrete subjected to generalized stresses.

Over the last 60 years a lot of research has been undertaken in order to formulate a set of formulas that describe the strength properties of concrete. So far this research has made remarkable progress, and are now at a point where a general consensus regarding the shape and properties of the failure surface for concrete has been reached.

Also a multitude of models have been proposed, spanning from the very simple ones suitable for manual calculations, to the very complex ones that need large computational facilities.

Today we now see a spreading use of high–strength, high–performance concrete, and the question arises whether or not we can predict the strength behavior of these new concretes using the models we have.

The problem revolves around the question of extrapolating the models based on $10 - 60$ MPa concrete, to include the new concretes with strengths of more than 100 MPa. It seems to be rather unsafe to extrapolate that much, and experimental data is therefore needed. Such an experimental program has been planned for the coming year at the Technical University of Denmark, as a part of a large research effort into high–strength, high–performance concrete.

However, prior to launching a major experimental program you have to sum up what the present state–of–the–art is. This in order not to spend a lot of time and money discovering things already known.

This report is part of this preparation in that it tries, partly to describe the consensus that has been reached regarding the properties of the failure surface, and partly to discuss the factors that affects, or is thought to affect, the multiaxial strength of concrete.

Chapter 2

FAILURE CRITERIA FOR CONCRETE UNDER SHORT TERM LOADING

A failure criterion is not, as the name suggest, a criterion for determining when a material fails, but rather a criterion for determining the peak loading capacity for a given material. Therefore the more appropriate term 'ultimate strength criterion' is sometimes used. However, in order not to confuse things the name 'failure criterion' will be used in this report.

In this chapter we shall first briefly discuss the derivation of the stress invariants, followed secondly by a section on the general properties of the failure surface, and finally we shall describe a number of the more important failure models that have been proposed over the years.

2.1 Stresses and stress invariants.

When proposing an ultimate strength criterion for concrete it is usually assumed that the concrete is a homogeneous and isotropic material. When the size of the aggregate is considerably smaller than the smallest size of the specimen considered, this is normally also the case. In the basic sense the ultimate strength of the concrete can then only be a function of the stresses, that is:

$$f(\sigma_{ij}) = 0 \tag{2.1}$$

since the stresses, σ_{ij}, can be uniquely described by the principal stresses σ_1, σ_2, σ_3, and the principal vectors n_1, n_2, and n_3, the failure criterion can the be written as:

$$f(\sigma_1, \sigma_2, \sigma_3, n_1, n_2, n_3) = 0 \tag{2.2}$$

Because we have initially assumed the concrete to be isotropic, the failure criterion must therefore be independent of the principal vectors, and eq.(2.2) resolves to:

$$f(\sigma_1, \sigma_2, \sigma_3) = 0 \tag{2.3}$$

It has been shown, i.e. in [89.2], that instead of expressing the failure criterion as a function of the principal stresses, eq.(2.3), the failure criterion can be expressed as a function of the 3 principal stress invariants I_1, J_2, and J_3, that is:

$$f(I_1, J_2, J_3) = 0 \tag{2.4}$$

2.1.1 Stress invariants

Consider a stress field given by:

$$\sigma_{ij} = \begin{bmatrix} \sigma_x & \tau_{xy} & \tau_{xz} \\ \tau_{yx} & \sigma_y & \tau_{yz} \\ \tau_{zx} & \tau_{zy} & \sigma_z \end{bmatrix} \tag{2.5}$$

The principal stresses can then be found as the solution to:

$$|\sigma_{ij} - \sigma\delta_{ij}| = 0 \tag{2.6}$$

which gives a cubic equation in σ:

$$\sigma^3 - I_1\sigma^2 + I_2\sigma - I_3 = 0 \tag{2.7}$$

In this equation the roots are the principal stresses σ_1, σ_2, and σ_3, and I_1, I_2, and I_3 are called the invariants of the stress tensor, which are defined by:

$$I_1 = \sigma_{ii} = \sigma_x + \sigma_y + \sigma_z \tag{2.8}$$

$$I_2 = \sigma_x\sigma_y + \sigma_y\sigma_z + \sigma_z\sigma_x - \tau_{xy}^2 - \tau_{xz}^2 - \tau_{zx}^2 \tag{2.9}$$

$$I_3 = \begin{bmatrix} \sigma_x & \tau_{xy} & \tau_{xz} \\ \tau_{yx} & \sigma_y & \tau_{yz} \\ \tau_{zx} & \tau_{zy} & \sigma_z \end{bmatrix} \tag{2.10}$$

A more simple form of these invariants can be found by using the definition that the shear stresses equals zero in the plane defined by the principal vectors. Therefore eq.(2.8) – (2.10) resolves to:

$$I_1 = \sigma_1 + \sigma_2 + \sigma_3 \tag{2.11}$$

$$I_2 = \sigma_1\sigma_2 + \sigma_2\sigma_3 + \sigma_3\sigma_1 \tag{2.12}$$

$$I_3 = \sigma_1\sigma_2\sigma_3 \tag{2.13}$$

The stress field defined by σ_1, σ_2, and σ_3 can be split into two parts, namely a 'hydrostatic' stress field and a 'deviatoric' stress field. The hydrostatic stress field is defined as the stress field where:

$$\sigma_m = \frac{1}{3}(\sigma_1 + \sigma_2 + \sigma_3) = \frac{1}{3} I_1 \tag{2.14}$$

and the deviatoric stress field is therefore defined by:

$$s_{ij} = \sigma_{ij} - \sigma_m \delta_{ij} \tag{2.15}$$

Similar to the invariants of the stress tensor, we can derive the invariants of the deviatoric stress tensor by solving the equation:

$$|s_{ij} - s\delta_{ij}| = 0 \tag{2.16}$$

and we get the invariants of the deviatoric stress tensor as:

$$J_1 = s_1 + s_2 + s_3 = 0 \tag{2.17}$$

$$J_2 = \frac{1}{2}(s_1^2 + s_2^2 + s_3^2) = \frac{1}{6}[(\sigma_1 - \sigma_2)^2 + (\sigma_2 - \sigma_3)^2 + (\sigma_3 - \sigma_1)^2] \tag{2.18}$$

$$J_3 = \frac{1}{3}(s_1^3 + s_2^3 + s_3^3) = s_1 s_2 s_3 \tag{2.19}$$

where:

$$\begin{bmatrix} s_1 \\ s_2 \\ s_3 \end{bmatrix} = \begin{bmatrix} \sigma_1 - \sigma_m \\ \sigma_2 - \sigma_m \\ \sigma_3 - \sigma_m \end{bmatrix} \tag{2.20}$$

2.1.2 General interpretation of the stress invariants.

The failure criterion is a surface in a cartesian coordinate system with the axes σ_1, σ_2, and σ_3. Any point, P, on the failure surface can alternatively to using the normal cartesian coordinates, be described by the two vectors, $\overline{ON}$, and $\overline{NP}$, and the angle θ, as shown in Fig.2.2.

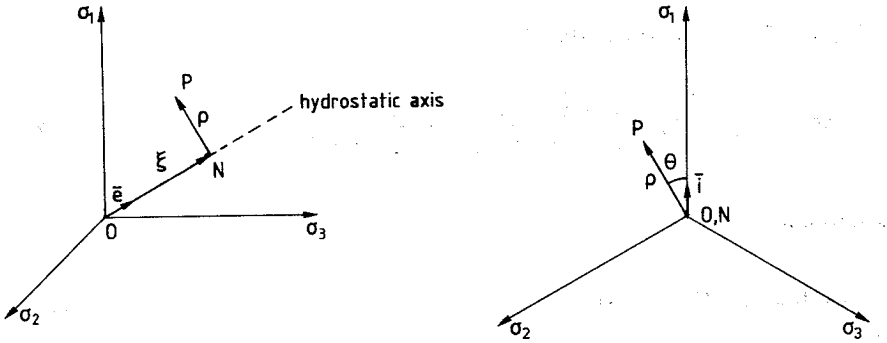

Fig. 2.1: Describing a point in space by 2 vectors and an angle.

The vector $\overline{ON}$ is lying on the hydrostatic axis, and its length, ξ, is:

$$\xi = |\overline{ON}| = \overline{OP} \cdot \bar{e} = [\sigma_1 \ \sigma_2 \ \sigma_3] \cdot \frac{1}{\sqrt{3}} \begin{bmatrix} 1 \\ 1 \\ 1 \end{bmatrix} = \frac{1}{\sqrt{3}} I_1 \qquad (2.21)$$

Perpendicular to the hydrostatic axis we have the deviatoric plane. In this plane we have a unit vector $\bar{i}$ situated along the projection of the σ_1–axis, with the definition:

$$\bar{i} = \frac{1}{\sqrt{6}} [2 \ -1 \ -1] \qquad (2.22)$$

The vector $\overline{NP}$ is defined by:

$$\overline{NP} = \overline{OP} - \overline{ON} = [\sigma_1 \ \sigma_2 \ \sigma_3] - [\sigma_m \ \sigma_m \ \sigma_m] = [s_1 \ s_2 \ s_3] \qquad (2.23)$$

and the length of $\overline{NP}$, ρ, is therefore:

$$\rho = \sqrt{|\overline{NP}| \cdot |\overline{NP}|} = \sqrt{s_1^2 + s_2^2 + s_3^2} = \sqrt{2 \cdot J_2} \tag{2.24}$$

The angle θ is determined by:

$$\overline{NP} \cdot \overline{1} = \rho \cos\theta \tag{2.25}$$

using eq.(2.22) and (2.24) we then get:

$$\cos\theta = [s_1 \; s_2 \; s_3] \cdot \frac{1}{\sqrt{6}} \begin{bmatrix} 2 \\ -1 \\ -1 \end{bmatrix} \cdot \frac{1}{\sqrt{2 \cdot J_2}} = \frac{2\sigma_1 - \sigma_2 - \sigma_3}{2\sqrt{3}\sqrt{J_2}} \tag{2.26}$$

and by using:

$$\cos 3\theta = 4\cos^3\theta - 3\cos\theta \tag{2.27}$$

we finally get:

$$\cos 3\theta = \frac{3\sqrt{3}\, J_3}{2\, J_2^{3/2}} \tag{2.28}$$

Another way of using eq.(2.27), is to compare this identity with eq.(2.7) and eq.(2.16). By doing so we can define the three principal stresses of s_{ij} and σ_{ij} as, see Chen [82.3]:

$$\begin{bmatrix} s_1 \\ s_2 \\ s_3 \end{bmatrix} = \begin{bmatrix} \sigma_1 \\ \sigma_2 \\ \sigma_3 \end{bmatrix} - \begin{bmatrix} \sigma_m \\ \sigma_m \\ \sigma_m \end{bmatrix} = \frac{2}{\sqrt{3}} \sqrt{J_2} \begin{bmatrix} \cos\theta \\ \cos(\theta - 2\pi/3 \\ \cos(\theta + 2\pi/3 \end{bmatrix} \tag{2.29}$$

for

$$0 \le \theta \le \frac{\pi}{3} \tag{2.30}$$

which means that the failure surface can be described in the form:

$$f(I_1, J_2, \theta) = 0 \tag{2.31}$$

2.1.3 Octahedral stresses.

Due, partly to their physical interpretation, and partly to their widespread use, the octahedral stresses are worth mentioning.

Consider a plane whose normal makes equal angles with each of the principal axis. This plane is called the octahedral plane, and the normal has the form:

$$n_i = [n_1 \;\; n_2 \;\; n_3] = \frac{1}{\sqrt{3}} [1 \;\; 1 \;\; 1] \tag{2.32}$$

The normal stress, σ_{oct}, on this plane is given by:

$$\sigma_{oct} = \sigma_1 n_1^2 + \sigma_2 n_2^2 + \sigma_3 n_3^2 = \frac{1}{3}(\sigma_1 + \sigma_2 + \sigma_3) = \frac{1}{3} I_1 \tag{2.33}$$

The shear stress, τ_{oct}, on this plane is given by:

$$\begin{aligned} \tau_{oct}^2 &= (\sigma_1 n_1)^2 + (\sigma_2 n_2)^2 + (\sigma_3 n_3)^2 - \sigma_{oct}^2 \\ &= \frac{1}{3}(\sigma_1^2 + \sigma_2^2 + \sigma_3^2) - \frac{1}{9}(\sigma_1 + \sigma_2 + \sigma_3)^2 \\ &= \frac{1}{9}[(\sigma_1 - \sigma_2)^2 + (\sigma_2 - \sigma_3)^2 + (\sigma_3 - \sigma_1)^2] \end{aligned} \tag{2.34}$$

Using eq.(2.18) we get:

$$\tau_{oct} = \sqrt{\frac{2}{3} J_2} \tag{2.35}$$

The failure surface can then be described by:

$$f(\sigma_{oct}, \tau_{oct}, \theta) = 0 \tag{2.36}$$

2.2 Properties of the failure surface.

One advantage of using eq.(2.31) instead of eq.(2.3), is that eq.(2.3) requires knowledge about the principal stresses σ_1, σ_2, and σ_3 before you can determine the failure surface, whereas eq.(2.31) gives you the failure surface explicitly when you know the stress field.

The advantage lies primarily in that you do not have to solve the eigenvalue problem of determining the principal stresses on basis of the stress field, when using eq.(2.31) instead of eq.(2.3).

2.2.1 The failure surface in the deviatoric plane.

Another, and probably more interesting, advantage of eq.(2.31) as compared to eq.(2.3) is that some interesting properties of the failure surface appears.

The cos–function is periodic with a period of 2π. It follows from eq.(2.28) that the failure surface in the deviatoric plane must then be periodic with a period of $2\pi/3$. Furthermore, since $\cos(3\theta) = \cos(-3\theta)$, the failure surface must be symmetric about $\theta = 0$.

In addition, if we set $\theta = \psi + \pi/3$ we get $\cos(3\theta) = \cos(3\psi + \pi) = -\cos(3\psi) = -\cos(-3\psi)$, we get that the failure surface, for $0 \leq \theta \leq 2\pi/3$, is symmetric about $\theta = \pi/3$. The conclusion is that the failure surface is explicitly defined by the interval $0 \leq \theta \leq \pi/3$.

Note that these arguments and conclusions regarding the shape of the failure surface are only true when the concrete is considered isotropic, but this is normally also the case, as mentioned earlier in this chapter.

2.2.2 Development of the failure surface along the hydrostatic axis.

The development of the failure surface is best described by the cross sectional shape of the surface in the deviatoric plane and by the meridians. A meridian is an intersection curve between the failure surface and a plane (meridian plane) containing the hydrostatic axis. The meridian plane is defined by a given value of θ. Three meridians are worth mentioning:

Tensile meridian	$\theta = 0^{\circ}$
Shear meridian	$\theta = 30^{\circ}$
Compressive meridian	$\theta = 60^{\circ}$

Tensile meridian

The stress state consists of a hydrostatic stress with a tensile stress superimposed in one direction. The resulting stress state is therefore as follows:

$$\sigma_1 = \sigma_2 < \sigma_3 \quad \text{tension positive} \tag{2.37}$$

The tensile meridian includes the uniaxial tensile strength, $(\sigma_1, \sigma_2, \sigma_3) = (0, 0, f_t)$, and the equal biaxial compressive strength $(\sigma_1, \sigma_2, \sigma_3) = (f_c, f_c, 0)$. Data on this meridian is rather scarce, due to the difficulty in applying tensile forces to the concrete.

Shear meridian.

A pure shear state exists when $(\sigma_1, \sigma_2, \sigma_3) = 1/2(\sigma_1 - \sigma_3, 0, \sigma_3 - \sigma_1)$. When this stress state is superimposed on a hydrostatic stress of $\sigma_1 = \sigma_2 = \sigma_3 = 1/2(\sigma_1 + \sigma_3)$ the resulting stress state is $(\sigma_1, \sigma_2, \sigma_3) = (\sigma_1, 1/2(\sigma_1 + \sigma_3), \sigma_3)$. The shear meridian is therefore defined by the following stress state:

$$\sigma_1 > \frac{1}{2}(\sigma_1 + \sigma_3) > \sigma_3 \quad \text{tension positive} \tag{2.38}$$

Compressive meridian.

Most of the tests so far lies on the compressive meridian. The compressive meridian consists of a compressive stress in one direction superimposed upon a hydrostatic stress state. This corresponds to:

$$\sigma_1 = \sigma_2 > \sigma_3 \quad \text{tension positive} \tag{2.39}$$

Data on this meridian includes the uniaxial compressive strength $(\sigma_1, \sigma_2, \sigma_3) = (0, 0, f_c)$, and the equal biaxial tensile strength $(\sigma_1, \sigma_2, \sigma_3) = (f_t, f_t, 0)$.

2.2.3 Characteristics of the failure surface.

Based on the mentioned symmetrical properties, the knowledge of the meridians, and the experimental results, the following general characteristics of the failure surface for concrete is indicated, see also Chen [82.3].

1/ The failure curve in the deviatoric plane is periodic with a period of $\pi/3$, and a starting value of 0.
2/ The failure curve in the deviatoric plane is smooth.
3/ The failure curve in the deviatoric plane is convex, at least for compressive stresses.
4/ The failure curve in the deviatoric plane has a shape as shown in principle in Fig. 2.2.

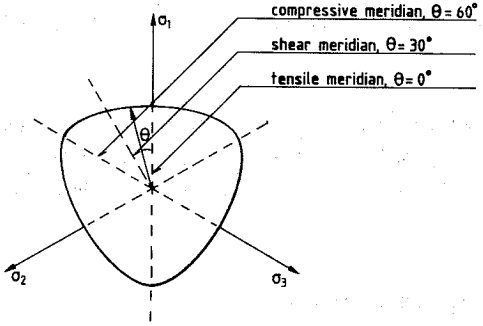

Fig. 2.2: *The failure surface in the deviatoric plane.*

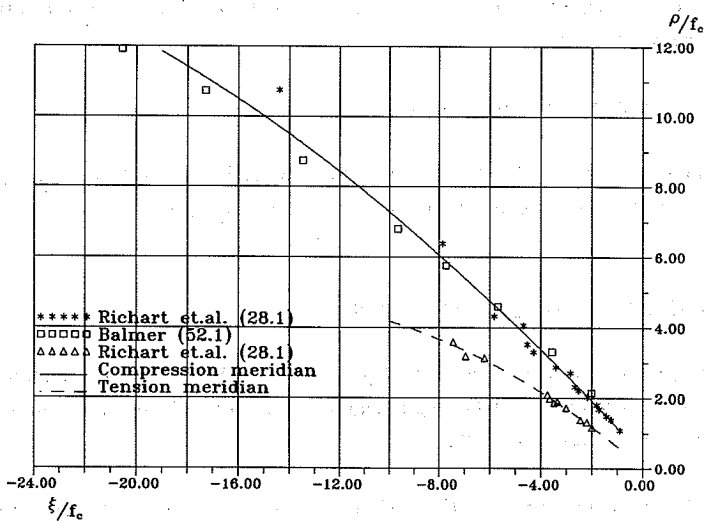

Fig. 2.3: *Test results on the compressive and tensile meridian.*

5/ The failure curve in the deviatoric plane is nearly triangular for tensile and small compressive stresses, and becomes more and more circular for higher compressive stresses.

6/ The failure surface is open ended, so that pure hydrostatic pressure cannot cause failure. Tests have been reported along the compressive meridian up to $I_1 = -79$ f_c, without any tendency for the meridian to approach the hydrostatic axis.

7/ The failure surface, when normalized by the uniaxial compressive strength, f_c, seems independent of f_c, when the stresses are compressive.

8/ The ratio ρ_{ten}/ρ_{com} increases from approximately 0.5 at low hydrostatic stresses, but remains less than unity.

2.3 Proposed failure criteria for concrete.

In the following section some of the more common failure criteria that have been proposed over the years will briefly be discussed.

2.3.1 One–parameter model.

Maximum Tensile Stress Criterion (Rankine).

This criterion was formulated in 1876 by Rankine, and states that failure takes place in a specimen when the maximum principal stress in a point inside the specimen reaches the tensile strength of the material. This regardless of the values of the other principal stresses. The failure surface is therefore described by the following 3 equations:

$$\sigma_1 = f_t\,, \quad \sigma_2 = f_t\,, \quad \sigma_3 = f_t \tag{2.40}$$

This surface will in the following be called 'the tension cutoff'. By using eq.(2.29) we can fully describe this failure surface by the parameters I_1, J_2, and θ in the following way:

$$f(I_1, J_2, \theta) = 2\sqrt{3}\sqrt{J_2}\cos\theta + I_1 - 3 f_t \tag{2.41}$$

or by the parameters ξ, ρ, and θ:

$$f(\xi, \rho, \theta) = \sqrt{2}\,\rho\cos\theta + \xi - \sqrt{3}\, f_t \tag{2.42}$$

In Fig. 2.4 this criterion is illustrated by showing the tensile and compressive meridians, together with the trace of the failure surface in the deviatoric plane.

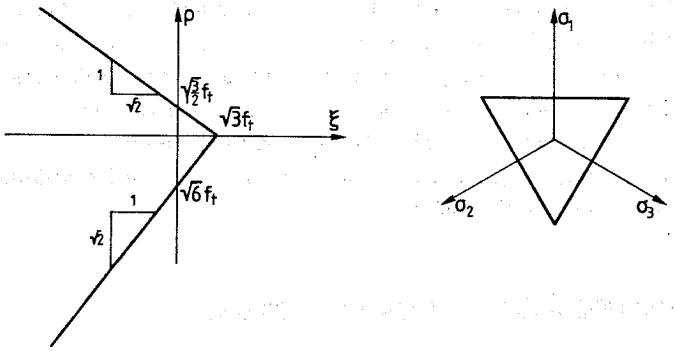

Fig. 2.4: *Failure surface defined by the Rankine maximum tensile stress criterion.*

2.3.2 Two–parameter models.

A number of two–parameter models have been proposed over the years. Among these are the Coulomb, the Mohr, the Mohr–Coulomb, and the Drucker–Prager criteria. Of these criteria, only the Mohr–Coulomb, and the Drucker–Prager criteria will be discussed here.

Mohr–Coulomb criterion.

The Coulomb criterion was formulated in 1773, and is in fact the first failure criterion proposed. For concrete the original Coulomb criterion has been modified, and is now called the Mohr–Coulomb criterion. This model enjoys a great popularity, partly due to the simplicity of the model, and partly because for the most cases of practical interest the model have an accuracy that is well within normal engineering accuracy.

The Mohr–Coulomb criterion is in fact a simplification of eq.(2.3), in that the effect of the intermediate principal stress, σ_2, is disregarded. This might seem to be an oversimplification, but the experimental evidence clearly show that the influence of σ_2 is very limited. The simplest criterion is then a linear relation between σ_1 and σ_3. In this model this relation is defined by:

$$k\sigma_3 - \sigma_1 - f_c = 0 \qquad \sigma_3 \geq \sigma_2 \geq \sigma_1 \tag{2.43}$$

For concrete the factor k is normally chosen to k = 4. If k is set to k = 1, eq.(2.43) reduces to Tresca's failure criterion which is often used for steel and other ductile materials. Using eq.(2.29) we get the failure surface as a function of I_1, J_2, and θ to:

$$f(I_1, J_2, \theta) = \frac{2}{\sqrt{3}}\sqrt{J_2}\,[k\cos\theta - \cos(\theta + \frac{2}{3}\pi)] + \frac{1}{3}(k-1)\,I_1 - f_c = 0 \qquad (2.44)$$

or as a function of ξ, ρ, and θ to:

$$f(\xi, \rho, \theta) = \sqrt{2}\,\rho\,[k\cos\theta - \cos(\theta + \frac{2}{3}\pi)] + (k-1)\,\xi - \sqrt{3}\,f_c = 0 \qquad (2.45)$$

The failure surface can then be shown as in Fig 2.5.

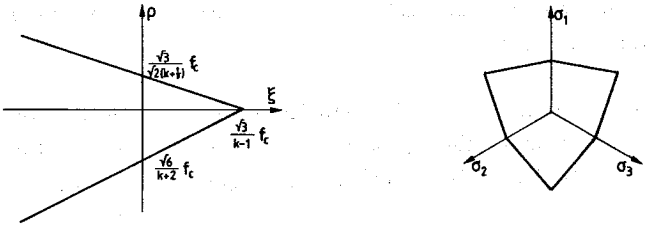

Fig. 2.5: *Failure surface defined by the Mohr–Coulomb failure criterion.*

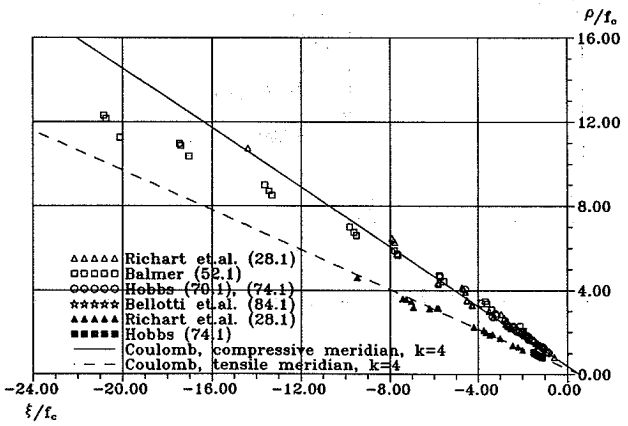

Fig. 2.6: *Mohr–Coulomb model compared with test data (cylinders).*

In Fig 2.6 the Mohr–Coulomb criterion is compared with test data from various workers. It is clear that the model corresponds well to the test data along both the meridians for hydrostatic loads less than $8 \cdot f_c$. In this region the model tends to be a little conservative, but the agreement is still very good. However, the model appears to be far too optimistic for higher hydrostatic loads. This is clearly because of the simplicity of the model in the assumption of linear meridians.

Tension–cutoff.

The Mohr–Coulomb failure criterion is most of the time used in conjunction with the so called tension–cutoff. The reason for this is when solving eq.(2.43) for the maximum tensile strength you get:

$$f_t = \frac{1}{k} f_c = \frac{1}{4} f_c \tag{2.46}$$

Since concrete does not have that much tensile strength, the tension–cutoff as defined by eq.(2.40) is introduced.

It should be noted, however, that introducing the tension–cutoff, the Mohr–Coulomb criterion changes into a three–parameter model. The effect of the tension–cutoff is best visualized by showing the failure surface for $(\sigma_1, \sigma_2, \sigma_3) = (0, \sigma_2, \sigma_3)$, as in Fig. 2.7.

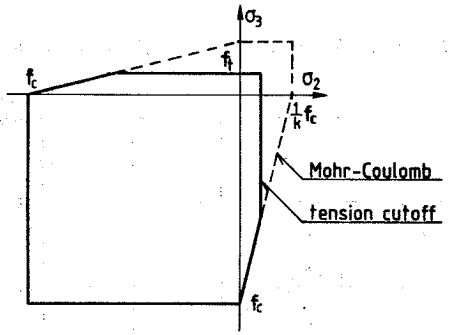

Fig. 2.7: Mohr–Coulomb failure surface with Tension–Cutoff, for biaxial stresses.

Drucker–Prager criterion.

The Mohr–Coulomb criterion is very suitable for problems where it is obvious which of the 6 sides of the hexagon is to be used. However the corners of the hexagon can cause difficulties in numerical applications of this model. A smooth approximation to the Mohr–Coulomb criterion has therefore been proposed by Drucker and Prager in the form:

$$f(I_1, J_2) = \sqrt{J_2} + \alpha I_1 - \beta = 0 \tag{2.47}$$

or

$$f(\xi, \rho) = \sqrt{6}\,\alpha\,\xi + \rho - \sqrt{2}\,\beta = 0 \tag{2.48}$$

The failure surface is a circular cone as shown in Fig. 2.8.

This model has shown to be fairly accurate when calibrated to fit the biaxial failure curve, except for tensile stresses. However the model in general gives poor results when used on triaxial stress fields. This is largely due to the two inherent properties of the model:

1/ The meridians are assumed linear, whereas triaxial test data clearly show that the meridians are curved, see fig. 2.3.
2/ The failure curve in the deviatoric plane is assumed always to be circular, which is only a close approximation for very large hydrostatic stress levels.

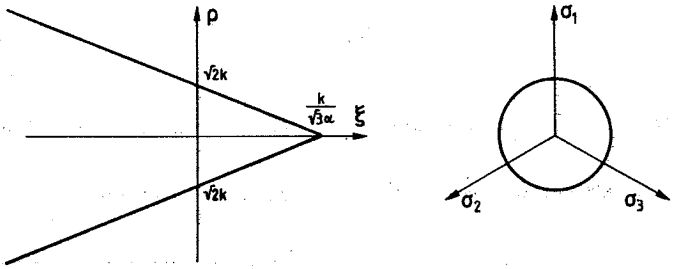

Fig. 2.8: Failure surface defined by the Drucker–Prager criterion.

2.3.3 Three–Parameter Model.

The previous mentioned failure models have been quite crude, since they assumed partly a linear relation between ξ and ρ, and partly that the failure surface in the deviatoric plane is either a circle, or composed of strait lines. The next logical step in modeling triaxial concrete behavior is therefore to change one of these two assumptions. The first step has been to change the shape of the failure surface in the deviatoric plane so to fit more closely to the experimental data, and in the meanwhile be smooth and convex.

Willam – Warnke Criterion.

Willam and Warnke have in 1975 proposed a model based on a linear relation between ξ and ρ, but having a smooth, convex, and non–circular failure surface in the deviatoric plane. The procedure used is that the deviatoric failure surface for $0 \leq \theta \leq 60^o$ can be considered as being a part of an elliptical curve, as shown in Fig. 2.9.

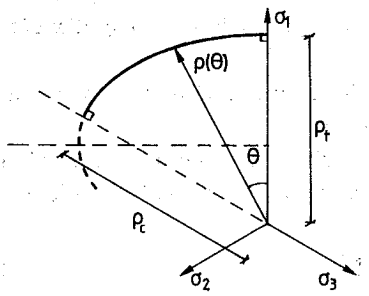

Fig. 2.9: The Willam–Warnke deviatoric failure surface for $0 \leq \theta \leq 60^o$

After some algebra, see Chen [82.3], the radius ρ can be described as:

$$\rho(\theta) = \frac{2\rho_c(\rho_c^2 - \rho_t^2)\cos\theta + \rho_c(2\rho_t - \rho_c)\sqrt{4(\rho_c^2 - \rho_t^2)\cos^2\theta + 5\rho_t^2 - 4\rho_t\rho_c}}{4(\rho_c^2 - \rho_t^2)\cos^2\theta + (\rho_c - 2\rho_t)^2} \qquad (2.49)$$

and:

$$\cos\theta = \frac{2\sigma_1 - \sigma_2 - \sigma_3}{\sqrt{2}\ \sqrt{6 \cdot J_2}} \tag{2.50}$$

The failure surface is then defined by:

$$f(\sigma_m, \tau_m, \theta) = \frac{1}{\alpha}\frac{\sigma_m}{f_c} + \frac{1}{\rho(\theta)}\frac{\tau_m}{f_c} - 1 = 0 \tag{2.51}$$

where

$$\sigma_m = \frac{1}{3} I_1 \quad \text{and} \quad \tau_m = \frac{2}{5} J_2 \tag{2.52}$$

The three parameters that needs to be determined is: ρ_c, ρ_t, and α. The parameters can be determined by the uniaxial compressive strength, f_c, the uniaxial tensile strength, f_t, and the equal biaxial compressive strength, f_{cc}. The results obtained are, see Chen [82.3]:

$$\alpha = \frac{f'_{cc} \cdot f'_t}{f'_{cc} - f'_t} \tag{2.53}$$

$$\rho_t = \sqrt{\frac{6}{5}}\ \frac{f'_{cc} \cdot f'_t}{2f'_{cc} + f'_t} \tag{2.54}$$

$$\rho_c = \sqrt{\frac{6}{5}}\ \frac{f'_{cc} \cdot f'_t}{3f'_{cc}f'_t + f'_{cc} - f'_t} \tag{2.55}$$

where

$$f'_{cc} = \frac{f_{cc}}{f_c} \quad \text{and} \quad f'_t = \frac{f_t}{f_c} \tag{2.56}$$

The failure surface can be illustrated as shown in Fig. 2.10.

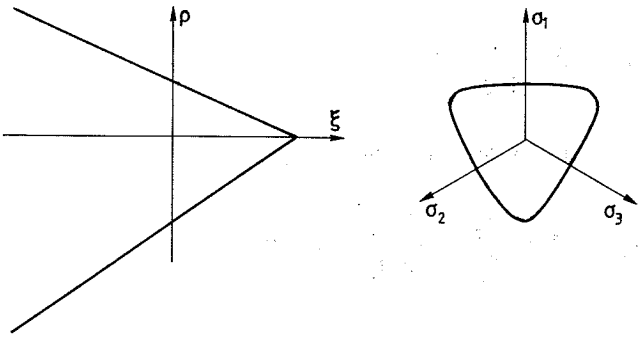

Fig. 2.10: Failure surface defined by the Willam – Warnke criterion.

The model is calibrated to the specific concrete by using results from test with low–order compressive and tensile stresses. It then follows that the model will yield good agreement with reality for stresses of the same magnitude, but due to the assumed linear relation between ξ and ρ the model does not catch the fact that at very high compressive stresses, the ratio ρ_t/ρ_c approaches unity.

Willam and Warnke have later modified this model so to include curved meridians. The resulting five–parameter model yields very good result, when compared to test data, however, you have to stop somewhere so this new model is not included in this report.

2.3.4 Four-Parameter Model.

The last logical step in the development of a failure criterion for concrete is to incorporate the nonlinear meridians. Ottosen [77.6] has suggested such a model.

Ottosen Criterion.

This criterion incorporates the 2 most important facts concerning a failure criterion for concrete.

1/ The meridians are curved, and smooth.
2/ The deviatoric cross section is smooth, curved, and convex, and develops from a nearly triangular shape at low hydrostatic stresses, to a nearly circular shape for high hydrostatic stresses.

The proposed model has the form:

$$f(I_1, J_2, \cos 3\theta) = A\frac{J_2}{f_c^2} + \lambda\frac{\sqrt{J_2}}{f_c} + B\frac{I_1}{f_c} - 1 = 0 \qquad (2.57)$$

Here the meridians are determined by the two constants A and B, and the deviatoric cross section is determined by the function λ.

The formulation of the development of the deviatoric cross section is based upon a membrane analogy. The analogy used is that of a membrane simply supported along the sides of an equilateral triangle. When this membrane is subjected to a uniform pressure, the contour lines of the deflected membrane vary between an equilateral triangle and a circle. The development of the function λ, that describes this behavior of the contour lines, is long and tedious, and therefore only the final results will be given here. For further information see [89.2].

$$\lambda = \begin{cases} K_1\cos[\frac{1}{3}\arccos(K_2\cos 3\theta)] & \text{for } \cos 3\theta \geq 0 \\ K_1\cos[\frac{\pi}{3} - \frac{1}{3}\arccos(-K_2\cos 3\theta)] & \text{for } \cos 3\theta \leq 0 \end{cases} \qquad (2.58)$$

The parameters A, B, K_1, and K_2 is determined on basis of the following four test data:

1/ Uniaxial compressive strength, f_c.
2/ Uniaxial tensile strength, f_t.
3/ Equal biaxial compressive strength, f_{cc}.
4/ A point on the compressive meridian, normally $(\xi,\rho) = f_c(-5,4)$.

After some algebra the parameters A, B, K_1, and K_2 can be found using the following equations, where (ξ,ρ) corresponds to the point on the compressive meridian as mentioned above:

$$M = \frac{\frac{\xi}{f_c} + \sqrt{3}\frac{\rho}{f_c}}{\frac{\rho}{f_c} - \frac{1}{\sqrt{3}}} \qquad (2.59)$$

$$B = \frac{3\,\frac{\rho}{f_c}\,\frac{f_c^2}{f_t f_{cc}} - \sqrt{3}}{M + \frac{9\,\frac{\rho}{f_c}}{\frac{f_{cc}}{f_c} - \frac{f_t}{f_c}}} \tag{2.60}$$

$$A = -\frac{\sqrt{3} + BM}{\frac{\rho}{f_c}} \tag{2.61}$$

$$\lambda_c = \sqrt{3}\,(1 + A - \frac{B}{3}) \tag{2.62}$$

$$\lambda_t = \sqrt{3}\,(\frac{f_c}{f_{cc}} + 2B - \frac{f_{cc}}{f_c}\frac{A}{3}) \tag{2.63}$$

$$\lambda_t = K_1 \cos[\,\frac{1}{3}\,\mathrm{Arccos}(K_2)\,] \tag{2.64}$$

$$K_2 = \cos\left[3\,\mathrm{Arctan}\,\frac{2\,\frac{\lambda_c}{\lambda_t} - 1}{\sqrt{3}}\right] \tag{2.65}$$

Using the mentioned test data the values of the parameters will be as shown in table 2.1.

$\frac{f_t}{f_c}$	A	B	K_1	K_2
0.05	3.4042	6.7992	22.7670	0.9997
0.08	1.8076	4.0962	14.4863	0.9914
0.10	1.2759	3.1962	11.7365	0.9801
0.12	0.9218	2.5969	9.9110	0.9647

Table 2.1: Parameters for Ottosen's model, the values and their dependence on the ratio f_t/f_c.

From table 2.1, it can be seen that the parameters depend heavily upon the value of f_t/f_c. However, the resulting failure surface is much less sensitive to the change in the f_t/f_c–ratio. This have been shown in Fig. 2.11, where the difference is less then 5 % when compa-

red to $f_t/f_c = 0.10$.

It can also be seen from the figure that the failure surface corresponds very good to the test data for low hydrostatic stresses. However, the failure surface appears a little too conservative for higher hydrostatic loads. Since the ratio f_t/f_c is decreasing for increasing uniaxial concrete compressive strength it is indicated that the error in the model is increasing for increasing compressive strength. However, for all practical purposes the Ottosen model appears to have good correlation with approved test results.

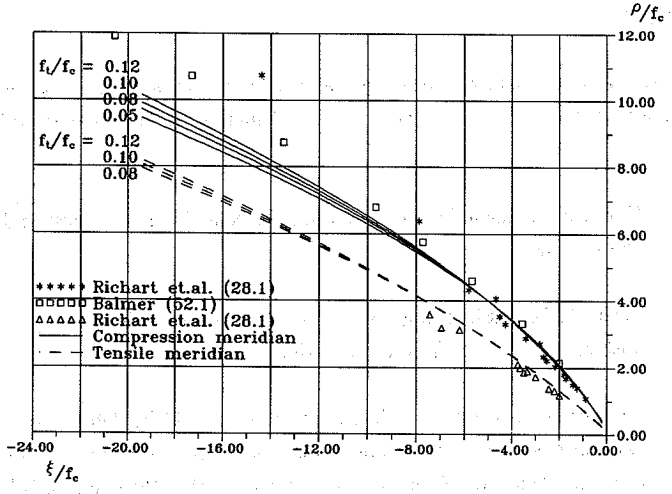

Fig. 2.11: Ottosen model compared to test data.

2.3.5 Other Criteria.

There exist a multitude of failure criteria for concrete other than the ones described here. Among these are the Tresca and the von Mises criteria, or the 5–parameter model of Willam and Warnke.

In this report it has been attempted to describe only some of the more important failure criteria for concrete, along with the development of failure criteria from the simpler ones suitable for manual calculations, to the more complex models requiring large computational facilities. In this process something has to be left out. However, the presented models gives a very good picture of the general consensus regarding the shape and properties of the failure surface, and further work would only tend to continue along the same beaten path.

Chapter 3

TESTING APPARATUS

In order to test concrete specimens under triaxial stress states a number of different test rigs have been used over the years. In this chapter a review over the most popular test rigs will be given.

It is clear that in order to get consistent, and reliable results there are some basic demands that have to be met by a given test rig. These demands can be summarized into the following:

1/ The test rig should be able to induce a specified uniform stress and strain state in the specimen.

2/ It should be possible to get accurate strain measurements from the test specimen, without interference from the test rig.

3/ The resultant stress state in the specimen should be determined only by simple calculations. This in order not to make assumptions about the stress distribution, or overall behavior of the material tested, i.e. that the material is linear–elastic.

4/ Low cost, and simplicity of operation.

Up until now most of the work in multiaxial testing have been performed on one of the following three different test specimens.

1/ Cubes, see Fig. 3.1.
2/ Massive cylinders, see Fig. 3.2.
3/ Hollow cylinders, see Fig. 3.3.

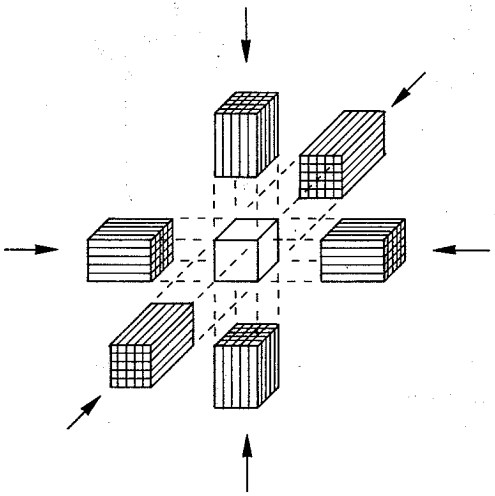

Fig. 3.1: *True triaxial test rig for cubes, brush platens.*

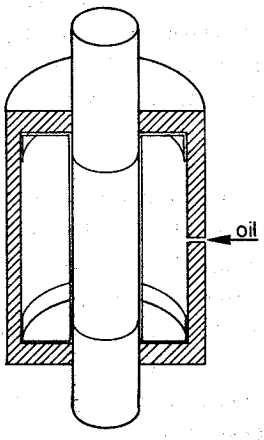

Fig. 3.2: *Triaxial cell for massive cylinders.*

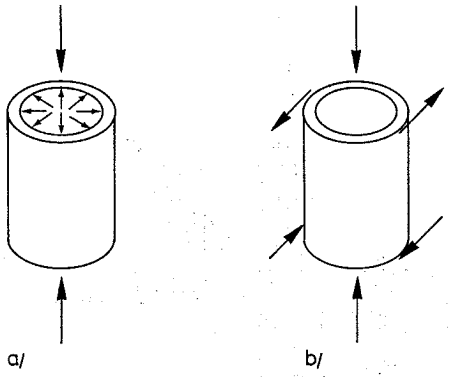

Fig. 3.3: *Hollow cylinders subjected to axial load, combined with:*
a: internal, or external pressure,
b: torsion.

3.1 Test rig for cubes.

The basic concept for this test rig is to load the opposing faces of a cube with a certain force. These forces are normally supplied by hydraulic jacks, see Fig. 3.1. The test rig has therefore the capability to generate a stress field inside the cube, where the principal stresses are independent of each other, that is, any combination of σ_1, σ_2, and σ_3 can be generated.

Test rigs for cubes fall into 2 categories: one–part, and multi–part machines. The difference is as follows. When a cube is loaded with a deviatoric stress, the cube will not strain in the same way along the three principal axis. When using a one–part machine the jacks are in a fixed position with respect to each other, and the concrete cube will therefore, due to its own deformations, be 'pushed into a corner'. This means that the faces of the cube no longer will be perpendicular to each other, and the stress state along one or more of the principal axis no longer will be uniform. In a multi–part machine, however, the jacks are not in a fixed position with respect to each other, but rather in a fixed position with respect to the particular face of the cube they are loading. In other words, they are free to follow the deformations of the cube so to ensure a uniform stress state in the concrete.

The next problem is transferring the forces from the jacks to the cube. When transferring the force, one must ensure that the test setup imposes no, or very little, restraint on the

concrete. Especially friction between the concrete and the load platens poses a major problem. Wang et.al. [87.1] reports it possible to get an ultimate strength reduction of 50% or more in biaxial tests, when reducing this friction by means of two teflon sheets with MoS_2–grease in between, as compared to using no interlayers. However, when using interlayers between concrete and load platens there is always the chance that instead of just eliminating friction you create a boundary condition that actually lowers the concrete strength below the ultimate strength, i.e. bulging of the concrete due to soft interlayers, see also section 4.4.1.

Many researchers have tried another approach. Instead of using teflon sheets they are using steel brushes to eliminate friction. The use of such brushes, however, creates another problem. When the filaments of the brush is much smaller than the maximum aggregate size, some of the filaments will inevitably strike the mortar between the coarser aggregate particles. Since in normal concrete the modulus of elasticity is appreciably larger for the aggregate than for the mortar it follows that the stress distribution along the cube side is not uniform. Furthermore an indeterminable stress distribution is produced in the concrete around the filament tip. Loading through brushes may therefore initiate failure close to the surface of the concrete and thereby lead to premature failure of the specimen.

The last major problem concerning the use of cubes, is how to measure the concrete strains. Since the load platens occupy all of the exterior of the cube, it is impossible to attach strain gauges directly unto the faces. Schickert et.al. [77.1], and other researchers have solved that problem by sawing groves in the cube face in which gauges are mounted. The groves are then later filled with cement paste. However the test results show without doubt, that the groves had a significant negative effect on the ultimate strength of the concrete.

All in all the multi–part cube test rig is a very versatile and important test rig. However the above mentioned problems and the very high cost of making such a machine, makes this type of test rig hard to establish and run properly.

3.2 Test rig for massive cylinders.

The most commonly used test rig is the one for massive cylinders. A sketch of such a test rig is shown in Fig. 3.2.

The triaxial cell is very simple in construction. A concrete cylinder is enclosed in a membrane, usually made of rubber, and inserted into a chamber. Inside the chamber axial load is supplied by means of a conventional testing machine, acting via rams. The lateral load is supplied by means of oil pressure. The reason for the membrane is to prevent any leakage of oil into the specimen, and thereby producing unwanted pore pressure.

The friction restraint from the rubber membrane is negligible, and if the cylinder has a height/diameter ratio greater than $2 - 2.5$, previous investigations by Newman [64.1] have shown that the central third of the specimen is almost unaffected by the end restraint of the loading platens, see also chapter 4.

However when using a test rig of this type, it is not possible to have the principal stresses $\sigma_1 \neq \sigma_2 \neq \sigma_3$, because two of the principal stresses will always be alike, and equal to the oil pressure. Only the following stress combinations are possible (tension positive):

a/	$0 > \sigma_3 = \sigma_2 > \sigma_1$	test along the compression meridian, all stresses compressive.
b/	$0 > \sigma_1 > \sigma_2 = \sigma_3$	test along the tensile meridian, all stresses compressive.
c/	$\sigma_1 > 0 > \sigma_2 = \sigma_3$	test along the tensile meridian, one stress tensile, two stresses compressive.

Test a/ is performed as described above. Tests b/ and c/ have a slightly modified end–plate system as shown in Fig. 3.4. In addition test c/ is performed on a waisted cylinder, also shown in Fig 3.4.

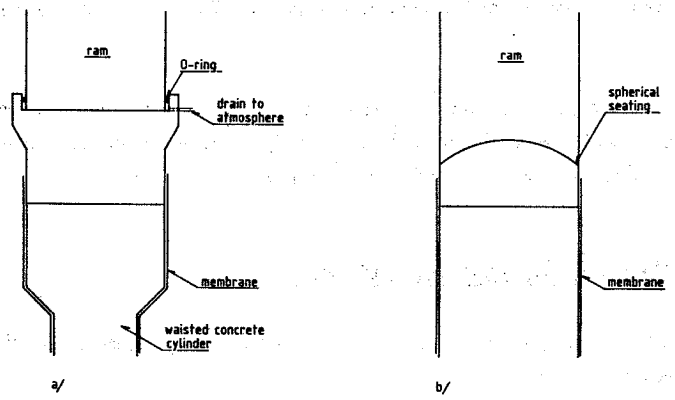

Fig. 3.4: End platens used in: a: test type b/ and c/, b: test type a/.

In tests b/ and c/ the end platen is modified so to fit over the ram, and is by means of a rubber O–ring sealed against the ingress of oil between the ram and the platen. To ensure that no pressure can build up between ram and end platen due to seepage of oil through the seal, a drain to the outside of the cell is also included. Using a normal cylinder it is then possible to supply an axial load lower than the oil pressure. Using waisted cylinders it is furthermore possible to get an axial tension, as in test c/. This is possible because the oil pressure will then, in addition to supplying the lateral stress, also supply an axial tension force on the shoulders of the concrete cylinder. This axial tension force can then be diminished by adding a compression force on the rams via the outside testing machine.

The strains are, in theory, quite simple to measure. This because the rubber membrane makes it possible to attach strain gauges directly on the concrete surface, without having to saw groves or the like in the concrete. There is naturally the chance that a crack will destroy a strain gauge on the concrete. It is therefore advisable to take measurements on any single gauge, rather than on a group of gauges.

In addition to the gauges, which measure local strains, it is also possible to measure the axial global strain of the concrete cylinder by measuring of the displacement of the ram. This displacement does of course also include the deformation of the ram, and the triaxial cell itself, but it should be possible to cancel out this deformation by making calibration tests as shown in Fig. 3.5.

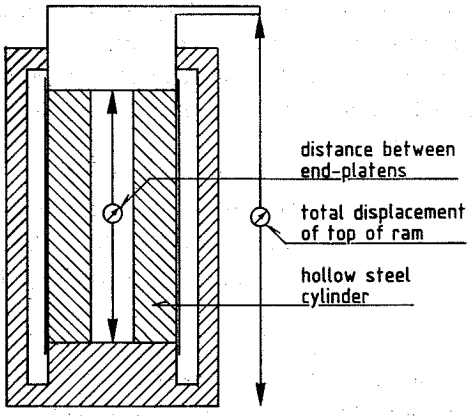

Fig. 3.5: *Calibrating equipment for axial global concrete strains.*

When a concrete cylinder is tested between any type of load platens, i.e. in the triaxial cell, the cylinder will deform as shown in Fig. 3.6.

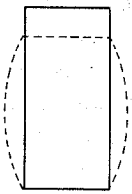

Fig. 3.6: Deformation of a concrete cylinder in a triaxial cell.

The reason for this barreling of the cylinder is the end restraint of the load platens. It is therefore obvious that measuring the global deformations will not give the correct strains in the concrete. However it is a good supplement to the strain gauges in case of the gauges being destroyed by cracks. Also due to the barreling any gauge should be placed in the middle third of the cylinder so the end restraint will have little or no influence on the measured strains.

3.3 Test rig for hollow cylinders.

A number of workers have created multiaxial stress fields by subjecting hollow cylinders to axial loads combined with either torsion or internal/external pressure as shown in Fig. 3.3. No objections to these tests can be raised as long as the results are <u>not</u> used to establish constitutive equations, failure criteria, or the likes for concrete. The reason for this rather forceful statement will appear below.

About the only positive things that can be said about performing triaxial tests on concrete this way, is that it requires less specialized test equipment, and the specimens are easier to mount gauges on. However a number of objections can be raised, and only the most serious will be mentioned here:

1/ In order to use the results obtained in these types of tests, it is necessary that the concrete used in the test is comparable to the normal everyday–concrete used in practice. This because several workers have shown that the basic properties of concrete changes with changing the mix design, i.e. the aggregate size.

When testing hollow cylinders you have to use a maximum aggregate size much smaller than wall size in order to be able to regard the concrete as being homogeneous. These two demands conflict, and no worker have solved them satisfactory.

2/ Several workers have assumed a uniform stress distribution. This is only valid as long as thin walled specimens, made of a homogeneous and isotropic material, are used. This clearly conflicts with the demands in 1/ because thin walled specimens require small aggregate, which again makes it difficult to relate the concretes used in the tests to the concretes of the real world.

3/ Since concrete does not fail plastically large stress gradients will occur across the cylinder wall. This means that failure is more likely to occur where these stresses have a maximum, unlike i.e. massive cylinders where failure is equally likely to occur anywhere in the specimen.

For these reasons results from tests on hollow cylinders will be discounted in this review.

Chapter 4

FACTORS THAT AFFECTS THE TRIAXIAL STRENGTH.

In this section a review will be given over the many different parameters or factors that affects, or is thought to affect, the triaxial strength of a concrete specimen.

4.1 Load path.

When raising the multiaxial load on a concrete specimen there are an infinite number of ways, load paths, to achieve this. The most commonly used load paths are as follows:

1/ Increasing the hydrostatic load to a specified level, $\sigma_1 = \sigma_2 = \sigma_3 = \sigma_m < 0$, and immediately hereafter applying a deviatoric stress so that:

$$\Delta\sigma_1 < 0 \quad \wedge \quad \Delta\sigma_3 = \Delta\sigma_2 = -\tfrac{1}{2}\Delta\sigma_1 \quad (\sigma_1 < \sigma_2 = \sigma_3) \quad \text{or}$$
$$\Delta\sigma_1 > 0 \quad \wedge \quad \Delta\sigma_3 = \Delta\sigma_2 = -\tfrac{1}{2}\Delta\sigma_1 \quad (\sigma_1 > \sigma_2 = \sigma_3)$$

2/ Similar to path 1, except that instead of immediately applying a deviatoric stress, the hydrostatic pressure is kept constant until the rate of increase of deformation is almost zero.

3/ Increasing the hydrostatic load to a specified level, $\sigma_1 = \sigma_2 = \sigma_3 = \sigma_m < 0$, and immediately hereafter either:

increasing σ_1 to failure, $\sigma_1 < \sigma_2 = \sigma_3$ or
decreasing σ_1 to failure, which occurs when either $\sigma_3 = \sigma_2 < \sigma_1 < 0$ or $\sigma_3 = \sigma_2 < 0 < \sigma_1$, depending on σ_m.

4/ A proportional load path, where $\Delta\sigma_1 = k_1\Delta\sigma_2 = k_2\Delta\sigma_3 < 0$, where k_1 and k_2 might be equal.

The load paths can be visualized as in Fig. 4.1.

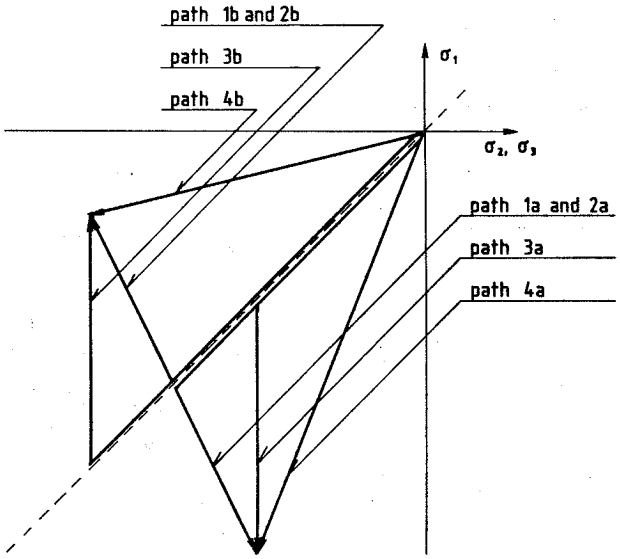

Fig. 4.1. *Different load paths for $\sigma_2 = \sigma_3$.*

It is widely known that the load path has an influence on the ultimate strength, although the size of that effect is disputed. Bazânt et.al. [80.2] claims that there exists very large difference between test using path 3 and 4, however, the illustration he is using to prove his point $(\sigma_1/f_c, \sigma_3/\sigma_1)$, $\sigma_1 < \sigma_2 = \sigma_3 < 0$ cannot be used to compare concretes of different strength. If instead the same test data is shown in a $(\sigma_1/f_c, \sigma_3/f_c)$ diagram, see Fig. 4.2, it is then clear that any significant difference between path 3 and 4 cannot be found.

Furthermore, due to comparison of different concretes, different test apparatus, and different curing conditions for the concretes it must be expected that the test data show a rather large variation. This makes it impossible, on basis of these tests, to determine whether or not the proportional load path results in a lower ultimate strength when compared to path 3.

Schickert et.al. [76.1] have made tests using load path 1 and proportional load path on almost identical concretes. The test results are shown in Fig 4.3 – 4.5. If anything can be concluded from these tests it is that the ultimate strength does not vary significantly when using path 1 and proportional load path, and when the concrete is only subjected to moderate confining pressures.

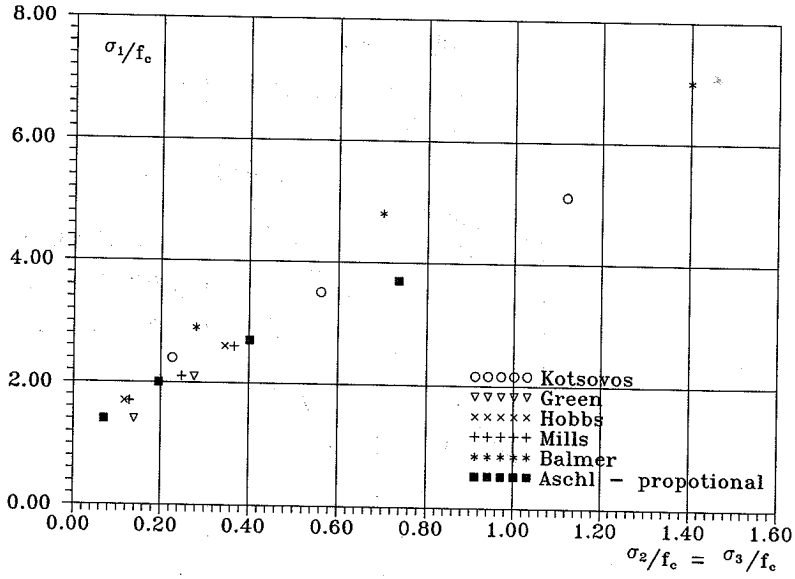

Fig. 4.2. *Comparison between load path 3a and proportional load path, after Bazant et.al. [80.2].*

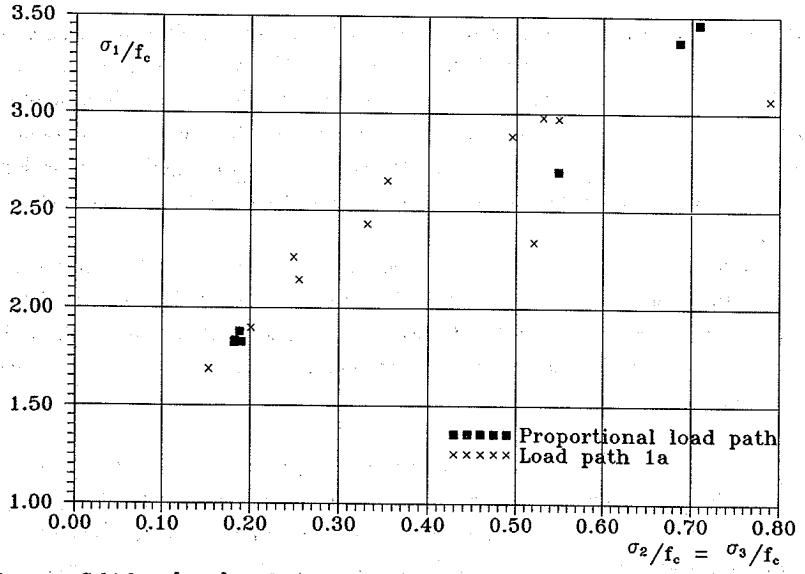

Fig. 4.3: *Schickert [76.1], path 1a versus proportional load path.*

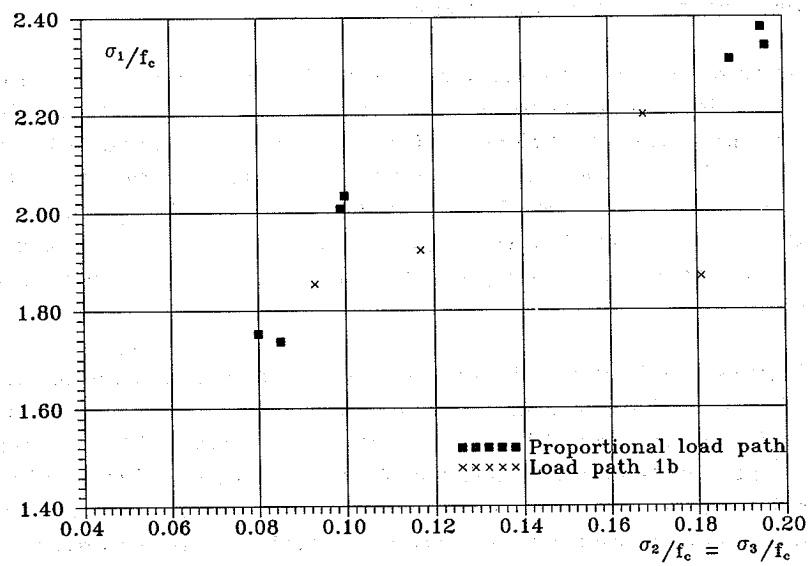

Fig. 4.4: Schickert [76.1], path 1b versus proportional load path.

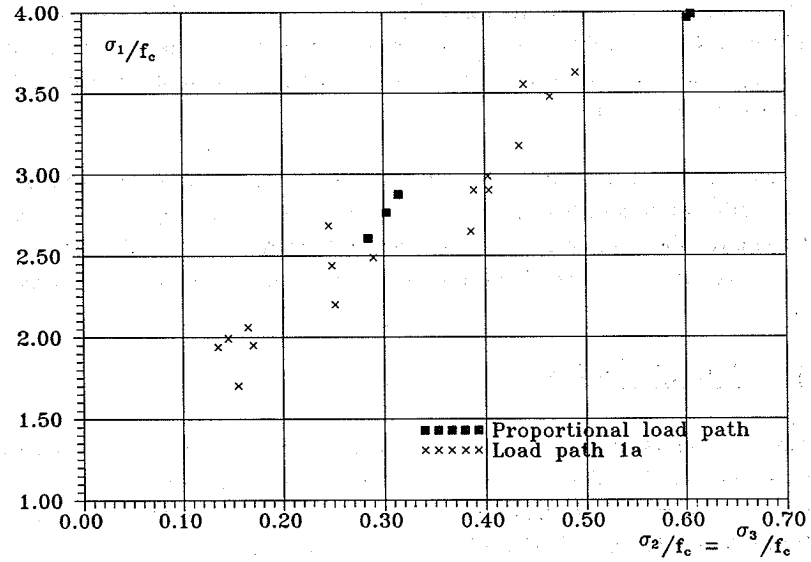

Fig. 4.5: Schickert [76.1], rough steel platens: path 1a versus proportional load path.

None of the above mentioned tests are conclusive though, because both authors have only compared tests with the minor stresses $\sigma_3 = \sigma_2 < f_c$.

Kotsovos, [79.4], made some comparison tests and concluded that although the ultimate strength is not greatly affected by the load path, for $\sigma_3 = \sigma_2 < 1.5 \cdot f_c$, the OSFP–level is very much affected. The OSFP–level (Onset of Stable Fracture Propagation) is when the microcracks in the concrete starts forming into larger and more coherent cracks. Kotsovos compared load path 1, 2 and 3, and found that load path 1 and 3 gave envelopes of the OSFP–level that were closed on the hydrostatic axis, whereas path 2 gave an open envelope, and finally that all envelopes where unaffected by the load path up to $\sigma_3 = \sigma_2 = 0.8 \cdot f_c$.

Kotsovos concluded that the difference observed is due to the formation of microcracks. It is so that the disruption which the concrete suffers from pure hydrostatic loads occurs in the form of microcracks, and the extents of these cracks increases with a/ increasing, and b/ sustaining the hydrostatic load. The microcracks are randomly located and oriented, and therefore acts as crack inhibitors when a crack, due to the later deviatoric stress, starts to propagate. This means that the microcracks tend to increase the energy required to start the failure process.

On basis of the above, Kotsovos concluded that the most critical load path must be a path where $\sigma_1 \leq \sigma_2 \leq \sigma_3 \leq 0$ at all times. Kotsovos have not made tests, nor collected tests, using proportional load path, so he only states that a proportional load path is the most simple path of this type.

If, however, you follow this augmentation, the conclusion must be that the most critical load path must be a path where there is the least amount of pure hydrostatic loading. This because you then quickly move outside the OSFP–envelope, and you therefore start to get more coherent crack systems in the concrete. This load path is the proportional load path.

4.2 Rate of loading.

There is a general consensus all over the world that the concrete strength is increased for increasing rate of loading. As a consequence of this most codes require a loading rate of a certain value when determining the uniaxial compressive strength. As an example the Danish National Standard, DS 423.23, requires a loading rate between 0.6 and 1.0 MPa/s.

The reason for requiring a certain loading rate is to exclude the influence of creep on the test results. However the difference in the uniaxial compressive strength has been found by Rüsch [60.3] not to be significant when the loading time ranges from some minutes to some hours.

In the reported triaxial tests the loading rate have been varied from approximately 0.05 MPa/s to 1.0 MPa/s, with ~0.3 MPa/s as the most commonly used loading rate. Especially the tests performed by Rossi [76.3] are important when discussing the effect of the rate of loading in triaxial tests. This because he did tests using loading rates of 0.05 and 1.0 MPa/s on identical concretes, and found that the results from the two different tests were not different in any significant way.

It is therefore concluded that when performing short term triaxial tests, the loading rate probably should not differ very much from the one used in determining the uniaxial compressive strength, so that the two results are readily comparable.

4.3 Pore pressure and saturated concrete.

If a concrete specimen is loaded by fluid pressure, and the fluid is free to penetrate into the concrete, pore pressure will develop. This is also the case when a specimen is loaded so to prevent the escape of pore water from inside the concrete.

4.3.1 Uncoated or unsealed concrete cylinders.

In the first case where the pressure fluid acts directly on the concrete, which is the case for submerged structures, pore pressure will develop in time as the fluid penetrates into the specimen.

If the pore pressure acts on an internal area, A_i, per unit concrete area, the reduction in the major, σ_1, and the minor, σ_3, principal stresses will be:

$$\sigma_{1,\text{true}} = \sigma_1 - A_i \cdot \sigma_{\text{pore}} \quad \text{and} \quad \sigma_{3,\text{true}} = \sigma_3 - A_i \cdot \sigma_{\text{pore}} \tag{4.1}$$

Butler [81.3] and others have shown, that for concrete close to failure A_i is approximately unity. Therefore when the fluid acts directly on the concrete surface the effective pore pressure will be roughly the same as the confining pressure.

If we insert eq.(4.1), for $A_i = 1$, into the Mohr–Coulomb failure criteria, eq.(2.43), we get:

$$k\sigma_{3,true} - \sigma_{1,true} - f_c = 0 \qquad \Leftrightarrow$$
$$\sigma_1 - \sigma_{pore} = k(\sigma_3 - \sigma_{pore}) - f_c$$

and since $\sigma_3 = \sigma_{pore}$

$$\sigma_1 - \sigma_3 = k\sigma_3 - k\sigma_3 - f_c \qquad \Leftrightarrow$$
$$\sigma_1 - \sigma_3 = -f_c \qquad (4.2)$$

This have been shown by Hobbs [81.2] to be a reasonable lower bound to test data from uncoated or unsealed concrete cylinders.

Akroyd [61.2] have also tested uncoated and unsealed cylinders, see Fig. 4.6. His results show a very good correlation with eq.(4.2). The reason for the observed difference is most probably due, partly to the relative low porosity of the 35 MPa concrete in that there was not time enough for the pore pressure to build up completely, and partly to A_i being less than 1.

4.3.2 Saturated, sealed cylinders.

In the second case pore pressure builds up due to the volumetric decrease of the cylinder. In structural concrete, water is usually free to drain, and it is therefore necessary to provide means for this in the test apparatus.

Akroyd [61.2] tested concrete cylinders cured as differently as oven–dried and submerged in water. His results show that for confining pressures below $\sigma_3 = f_c$ the ultimate strengths of the two concretes were approximately the same, however, for greater values of σ_3 the ultimate strength of the saturated concrete did not increase as much as the ultimate strength for the oven–dried concrete.

Kotsovos [78.1] and others have shown that the volume of the test specimen decreases at an increasing rate when subjected to increasing deviatoric stresses. This means that the resulting pore pressure in undrained tests also increases at an increasing rate, and that the

failure envelope for undrained tests with high deviatoric stresses should be markedly different from drained or oven–dried specimens, as in the tests of Akroyd.

Hobbs [70.1] have reported results showing that in drained and undrained tests the mean triaxial strengths were only significantly different on the 0.1% level. The concrete tested had a w/c–ratio of 0.47, was cured in a moist curing room, and tested with a confining pressure between 0 and $0.5 \cdot f_c$. The curing condition and mix design means that there was only a little free water left in the concrete. It is therefore likely that the pore pressure partly due to the lack of free water in the concrete, and partly due to the small volumetric strains, never grew large enough to influence the ultimate strength.

The conclusion must be that when testing concrete at higher confining pressures one should always allow for drainage. This, however, will probably not be enough when testing saturated specimens, because the water will not have time to drain at the same speed as the volumetric decrease due to the quickness of the load application. Therefore it must be recommended that the load application is slow, and the specimens are dry.

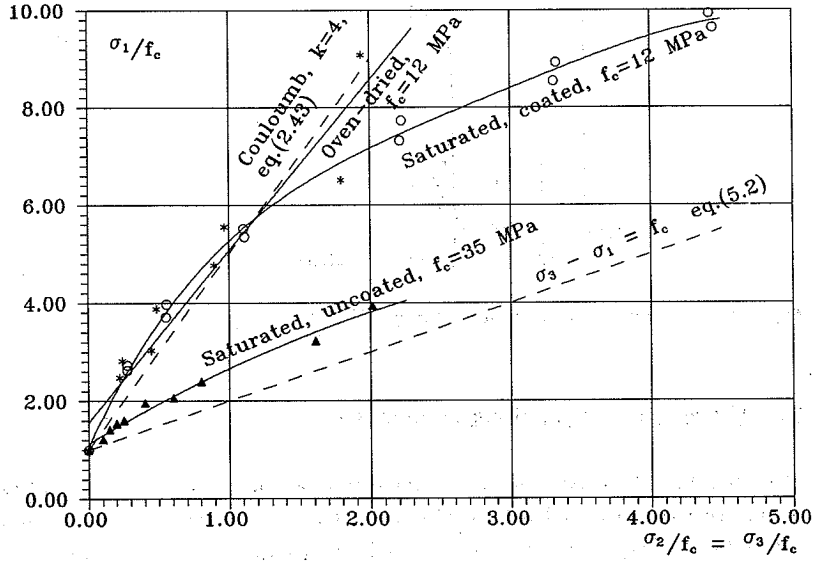

Fig. 4.6: *Akroyd [61.2], tests on oven–dried, saturated, and uncoated cylinders.*

4.4 Dimensions of the test cylinder.

4.4.1 Height/width ratio, and frictional end restraint.

Newman and Lahance [64.1] and Thaulow [60.1] have tested cubical and cylindrical test specimens in uniaxial compression with varying height/width ratio and various types of interlayers between the concrete and the press head. They agree that for height/width ratios between 2 and 2.5 a region of uniform stress exists in the middle third of the specimen, so this portion of a cylinder is unaffected by the end restraint.

Both workers also agree that the use of soft interlayers tend to reduce the concrete strength. This because when using soft interlayers, i.e. soft cardboard or rubber, the concrete tends to bulge out at the ends. This bulging creates tensile tangential stresses, and failure is therefore more likely to initiate at the ends rather than at mid height.

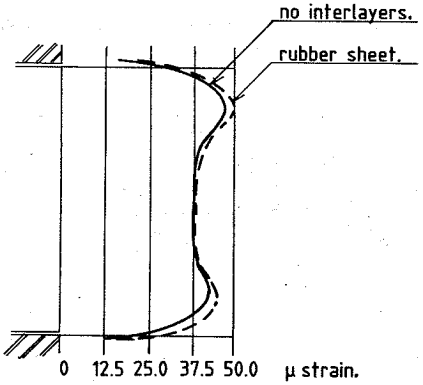

Fig. 4.7: Lateral deformations, using different interlayers.

4.4.2 Cylinder diameter/maximum aggregate size.

When selecting the maximum size of aggregate in a concrete it is necessary to take into account that the concrete has to be placed in a form. The dimensions of the form places a restraint on the aggregate size since the resulting material needs to be considered a homogeneous material.

Any wall in a form will influence the packing of the aggregates because the larger aggregates cannot pack as close along the wall as in the interior of the specimen. As a consequence of this the concrete along the wall has more mortar and less of the larger fraction of the aggregate. The mortar is normally stronger than the aggregate, this means that the use of large aggregates in small forms will result in the concrete being stronger along the wall than in the interior of the specimen. Due to this difference in strength, and due to the difference in aggregate content between the outer layer and the interior of the speciment it can therefore be difficult to consider the concrete homogeneous when using large aggregates in small forms.

Different codes and organizations recommends different limits to the ratio of the narrowest dimension of the form to the maximum aggregate size:

ACI 318, 1983	$D/d \geq 5$
BS 1881 part 3, 1970	$D/d \geq 4$
RILEM, 1956	$D/d \geq 4$
DS 423.21, 1984	$D/d \geq 3$
ASTM standard C192–76	$D/d \geq 3$

Normally when using massive cylinders a ratio of 4 is accepted as satisfactory.

When testing hollow cylinders or other thin walled specimens other limitations apply. A uniformly distributed stress field is generally assumed when test data from these specimens are treated. Due to the differences between the matrix material and the aggregate material, i.e. difference in Young's and Poisson's modulus, this assumption does not hold. It has been shown in [88.1] that these differences alone creates large variations in the stresses around the aggregates, and as a consequence the stresses in the specimen wall cannot be considered uniformly distributed. Therefore, when assuming a uniform stress field, it is evident, that the D/d ratio should be significant larger than the above mentioned recommendations, i.e. by at least a factor of $2-3$, see also Hobbs [73.1]

4.5 The aggregates in the concrete.

4.5.1 Absolute aggregate size.

It is a well known fact that the properties of concrete changes when the maximum aggregate size changes. This effect is most outspoken for richer mixes, i.e. high–strength con-

crete, see also [87.2] and [60.2]. The reason is that increasing the aggregate size results in lowering the bond area between aggregate and paste. As a consequence of this the larger aggregate particles will not be 'glued' as tight together by the cement paste as when using smaller aggregate sizes.

No quantitative assessments of the influence of the maximum aggregate size on the triaxial strength have yet been made. Therefore it must be recommended to use an aggregate size as close to the size used today in normal structural concrete.

4.5.2 Aggregate content.

Hobbs [74.1] and others have tested concretes with aggregate volume contents ranging from 0 to 75%, and f_c ranging from 15 to 57 MPa. The results are consistent with other workers, and reveals that the aggregate volume content has a positive influence on the ultimate triaxial strength.

Hobbs found that concretes or mortars with low aggregate content had a lower gain in strength and a more curved failure envelope than concretes with higher aggregate content. This effect got more pronounced when the uniaxial compressive strength decreased. Based on these findings the following approximation can be made:

No significant effect exist when:

$f_c \geq 30$ MPa: $V_{aggr} > 0.4$

$f_c \leq 30$ MPa: $V_{aggr} > 0.65$

In order to compare results from different sources, it is therefore necessary to establish V_{aggr} for the concretes compared, especially for low strength concretes.

4.5.3 Normal and heavyweight concrete.

Normally it is not possible to determine the properties of the type of aggregates used in the published results. However, Berra [84.7] have made test using aggregates as different as normal alluvial aggregate and very heavy barytes. These test show almost no difference between the ultimate triaxial strengths of the two concretes for confining pressures in the range $0 \leq \sigma_3 \leq f_c$

When comparing other tests using different aggregates over a wide range of uniaxial compressive strength, Balmer [52.1], Hobbs [70.1] and [74.1], Schickert [76.1], or Bellotti [84.1], it is seen that, apart from some expected scatter the tests show generally the same results. It is therefore unlikely that the type of aggregate, as long as it is not lightweight aggregate, has any significant effect on the multiaxial strength.

4.5.4 Lightweight concrete.

There have only been published very little work on lightweight concrete under multiaxial stresses. The most extensive work has been performed by Hansen [63.1] on a variety of aggregates, but also Hobbs [81.2] and Berra [84.7] have tested lightweight concretes, see Fig. 4.8.

The main conclusion of all the workers is that the type of lightweight aggregate used has a decisive influence on the failure envelope. Comparing the tests with the Mohr–Coulomb failure criterion eq.(2.43) you get a k–factor of 4 for normal– and heavyweight concrete, whereas the lightweight concretes exhibits a much larger scatter in the results. The scatter is so large that it is not possible to determine a global k–factor for these concretes. As a lower bound solution k may be set to 1.5 for σ_3 in the range $0 \leq \sigma_3 \leq f_c$.

Berra [84.7] have stated that the failure criteria is depending on the porosity of the material. When compared with the Hansen tests such a conclusion could be possible. However, the porosity for the aggregates used in the Hansen test have not been measured, and it is therefore not possible at this time to give a closer evaluation of Berra's conclusion due to the lack of data.

As a conclusion the following equation, (4.3), can be used as a failure criterion for most lightweight concretes, but for the more extreme concretes this failure criterion is not applicable.

$$\sigma_1 = k\sigma_3 - f_c, \quad k = 1.5, \quad 0 \leq \sigma_3 \leq f_c \tag{4.3}$$

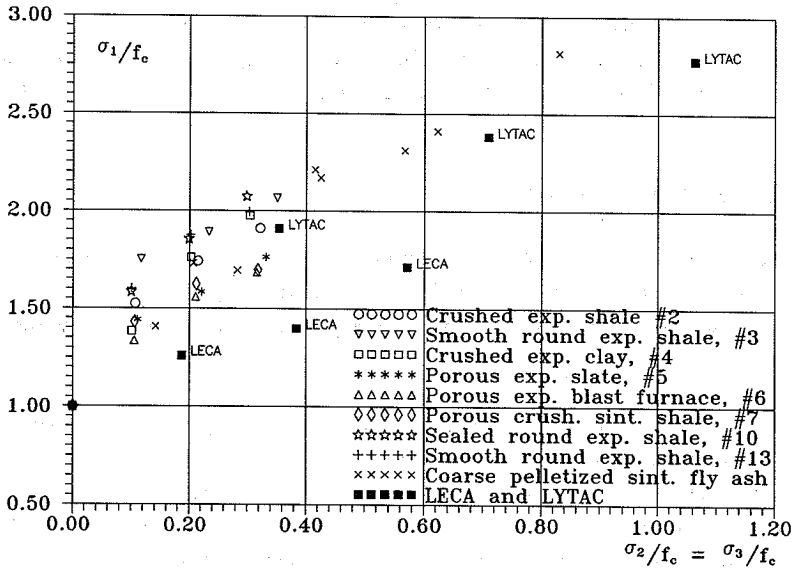

Fig. 4.8: *Hansen, Hobbs, Berra: lightweight concretes using different aggregates.*

4.6 The uniaxial compressive strength of the concrete.

Every worker agree that the most singular important factor in the ultimate triaxial strength of concrete is the uniaxial compressive strength. In Fig. 4.9 some test results along the compressive meridian are shown. All the plotted results are from cylinders 100·200 mm or 150·300 mm, and the concretes have been subjected to almost the same curing conditions.

It can be seen from the graph that, when the principal stresses are normalized with respect to f_c, the failure criterion can be expressed by a single equation regardless of the value of f_c. However two of the test series show a slightly larger triaxial strength, namely Balmer, f_c= 25 MPa, and Richart et.al. f_c = 7 MPa, but since the rest of the tests are in excellent agreement for f_c ranging between 18 and 56 MPa the most likely cause is probably that it is some other factor than f_c that is the cause of this larger triaxial strength. However it cannot completely be ruled out that there will be some difference in the triaxial strength of low–strength and high–strength concretes.

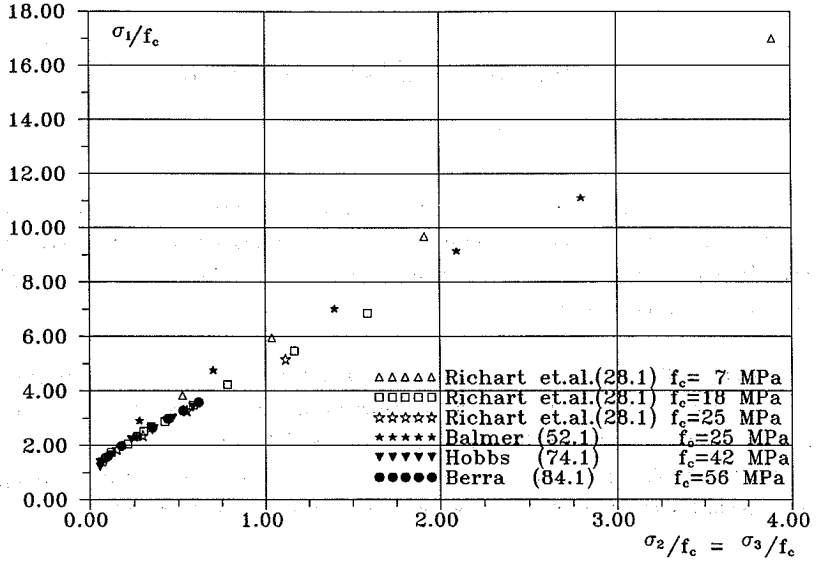

Fig. 4.9: *Triaxial test results on cylinders, varying uniaxial strength.*

Chapter 5

PREVIOUS INVESTIGATIONS

In this section most of the strength results from previous work have been compiled. Only work which have been performed on cubical or massive cylinder specimens have been included. This is due to the many problems concerning use of hollow cylinders, as described in chapter 3.

Also test results on cubes using solid load platens, with no attempt to reduce friction between concrete and steel, have been disregarded. This because it have been shown, i.e. by Schickert and Winkler [77.4], that the use of such platens creates very large restraints on the specimens, and results in an increase in the triaxial strength. In some reports increase in strength of more than 50% have been reported.

For each test series the following is noted:

1/	Specimen	The specimen type and size used in the tests.
2/	Storage	How the specimens were stored and cured before testing.
3/	Load path	Which load path the specimens were subjected to.
4/	V_{aggr}	V_{aggr} is the volume of the aggregate compared to the total volume of the concrete.
5/	Special	How friction between load platens and concrete was reduced in tests on cubes. Other information which is relevant, and particular, to the reported data, i.e. for cube tests: one–part or multi–part test rig, see also chapter 3.

For all the test results presented here the sign convention that compressive stresses are positive has been adopted.

5.1 Richart, Brantzaeg and Brown [28.1].

Specimen: Cylinder 100×200.

Storage: 28 day in moist, 1 day in dry condition.

Load path: Hydrostatic load until specified level, hereafter increasing σ_1 until failure.

V_{aggr}: ≈0.75

Spec. no.	f_c MPa	σ_1 MPa	$\sigma_2 = \sigma_3$ MPa
112	17.7	24.7	1.2
122		38.7	3.8
123		35.8	3.8
124		33.8	3.8
132		48.9	5.4
133		42.4	5.4
134		41.9	5.4
142		52.7	7.5
143		50.7	7.5
151		61.3	10.4
153		60.0	10.4
154		61.2	10.4
161		79.3	13.9
163		73.4	13.9
164		72.7	13.9
173		97.2	20.7
174		97.0	20.7
182		122.3	28.2
184		121.3	28.2
221	25.2	46.9	3.8
222		47.0	3.8
223		47.1	3.8
224		45.7	3.8
241		58.4	7.5
242		57.2	7.5
243		60.2	7.5
244		62.0	7.5
261		83.7	13.9
263		81.5	13.9
264		82.0	13.9
283		130.9	28.2
284		129.2	28.2

Spec. no.	f_c MPa	σ_1 MPa	$\sigma_2 = \sigma_3$ MPa
322	7.2	29.2	3.8
323		27.4	3.8
324		26.5	3.8
341		44.0	7.5
342		43.6	7.5
343		43.4	7.5
344		42.2	7.5
361		70.2	13.9
362		69.3	13.9
364		71.0	13.9
383		123.0	28.2

Specimen: 1: 100·200 mm cylinder

2: 100·560 mm cylinder

Load path: Axial load was applied first, hereafter oil pressure raised until failure.

Spec. no.	Spec. type	f_c MPa	σ_1 MPa	$\sigma_2 = \sigma_3$ MPa
E11	2	14.8	4.2	22.1
E14		15.2	4.2	36.7
E13		16.7	6.5	30.5
E20		13.5	6.4	47.6
31	1	5.8	4.5	26.9
32		5.0	8.6	36.7
34		5.5	4.5	25.7
35		6.7	8.6	37.9
37		7.7	4.5	25.7
38		6.7	8.3	36.7
39		8.6	11.7	49.5
40		9.4	4.5	27.4
41		7.8	8.0	37.9
42		8.3	11.7	44.1
51		10.7	4.7	32.2
54		12.6	4.7	34.1
57		14.5	4.7	35.3
60		16.7	4.7	32.9
61		17.0	8.2	47.0
77		25.8	5.0	46.5
80		25.6	5.0	41.7

5.2 Balmer [52.1].

Specimen: Cylinder 150·300 mm.
Storage: Fog cured for 28 days.
Load path: ?
V_{aggr}: ?

Spec. no.	f_c MPa	σ_1 MPa	$\sigma_2 = \sigma_3$ MPa
1	24.6	68.6	6.9
2		69.6	6.9
3		76.2	6.9
4		110.0	17.2
5		118.8	17.2
6		122.1	17.2
7		168.0	34.5
8		174.6	34.5
9		176.5	34.5
10		222.5	51.7
11		224.4	51.7
12		228.7	51.7
13		267.7	68.9
14		272.6	68.9
15		280.4	68.9
16		359.8	103.4
17		365.8	103.4
18		374.2	103.4
19		450.0	137.8
20		465.4	137.8
21		468.0	137.8
22		511.8	172.3
23		538.6	172.3
24		542.9	172.3

5.3 Gardner [69.1].

Specimen: Cylinder 75·150 mm.

Storage: 28 days under water, 28 days air cured, and then heated to 60°C for 48 hours.

Load path: ?

V_{aggr}: ? (ready–mix concrete).

Number of spec.	f_c MPa	σ_1 MPa	$\sigma_2 = \sigma_3$ M Pa
7	28.9	72.4	8.6
7		117.9	17.2
7		144.7	25.8

5.4 Hobbs [70.1].

Specimen: Cylinder 55·110 mm.

Storage: Moist curing room until testing.

Load path: Hydrostatic load until specified level, hereafter increasing σ_1, at 16 MPa/min, until failure.

V_{aggr}: 0.66.

Special: Test 1–6 are drained tests, where pore water is allowed to escape. Test 7–9 are undrained tests.

Test	f_c MPa	σ_1 MPa	$\sigma_2 = \sigma_3$ M Pa	age days
1	31.2	44.7	2.5	7
2		55.4	5.0	
3		76.0	10.0	
4		94.6	15.0	
7		41.7	2.5	
8		55.7	5.0	
9		91.7	15.0	
1	38.6	52.8	2.5	14
2		63.0	5.0	
3		86.6	10.0	
4		105.4	15.0	
7		50.9	2.5	
8		62.5	5.0	
9		102.8	15.0	
1	42.9	58.6	2.5	28
2		69.6	5.0	
3		94.8	10.0	
4		112.1	15.0	
5		128.9	20.0	
6		145.9	25.0	
7		52.3	2.5	
8		68.4	5.0	
9		109.9	15.0	
1	44.7	58.4	2.5	56
2		72.3	5.0	
3		96.1	10.0	
4		117.1	15.0	
5		137.9	20.0	
6		155.6	25.0	
7		56.1	2.5	
8		67.8	5.0	
9		115.7	15.0	

5.5 Mills and Zimmerman [70.2].

Specimen: 57 mm cubes.

Storage: Fog or water cured for 28 days, 1 month in air

Load path: Hydrostatic load until specified level, hereafter a deviator stress was applied. σ_1 and σ_2, was applied at a constant σ_1/σ_2 ratio.

V_{aggr}: > 0.6

Friction: Friction was reduced by using 2 teflon sheets with grease in between.

The test rig used was a one–part machine where the jacks are in a fixed position at all times during the test.

Spec no.	f_c MPa	σ_1 MPa	σ_2 MPa	σ_3 MPa
A1	23.0	53.1	5.8	5.8
A2		50.7	5.8	5.8
A3		57.9	11.6	5.8
A4		57.9	11.6	5.8
A5		53.1	17.4	5.8
A6		62.7	17.4	5.8
A7		65.1	23.2	5.8
A8		67.5	28.9	5.8
A9		67.5	34.7	5.8
A10		60.3	40.5	5.8
A11		56.8	47.8	5.8
A12		50.7	50.7	2.9
A13		77.2	67.5	8.7
A14		62.7	8.7	8.7
A15		72.4	14.5	8.7
A16		79.6	20.3	8.7
A17		79.6	26.1	8.7
A18		77.2	31.8	8.7
A19		82.0	37.6	8.7
A20		82.0	43.4	8.7
A21		82.0	49.2	8.7
A22		81.5	55.7	8.7
A23		82.0	60.8	8.7
A24		72.4	72.4	8.7
A25		41.0	2.9	2.9
A26		53.1	8.7	2.9
A27		53.1	14.9	2.9
A28		57.9	24.1	2.9
A29		55.5	20.3	2.9
A30		57.9	31.8	2.9

Spec no.	f_c MPa	σ_1 MPa	σ_2 MPa	σ_3 MPa
A31		55.5	37.2	2.9
A32		55.5	43.4	2.9
A33		57.9	49.3	2.9
A34		53.1	53.1	2.9
A35		43.4	2.9	2.9
A36		63.8	8.7	8.7
A37		65.1	63.8	5.8

Spec no.	f_c MPa	σ_1 MPa	σ_2 MPa	σ_3 MPa
B1	26.9	50.7	50.7	0.6
B2		45.8	45.8	0.6
B3		53.1	49.6	1.2
B4		50.7	50.7	1.2
B5		62.7	62.7	2.9
B6		62.7	62.7	2.9
B7		41.5	1.4	1.4
B8		41.7	2.9	2.9
B9		56.2	5.2	4.8
B10		61.5	5.2	4.8
B11		71.2	7.2	7.2
B12		71.1	7.2	7.2
B13		58.9	21.7	1.4
B14		66.1	36.2	2.9
B15		61.5	21.7	1.4
B16		68.8	28.9	2.9

Spec no.	f_c MPa	σ_1 MPa	σ_2 MPa	σ_3 MPa
C1	36.1	47.1	48.2	0.6
C2		51.6	53.1	0.6
C3		61.3	60.3	1.2
C4		51.2	50.7	1.2
C5		68.8	67.5	2.9
C6		68.3	66.6	2.9
C7		54.5	1.4	1.4
C8		59.3	2.9	2.9
C9		63.2	21.7	1.4
C10		72.8	28.9	2.9
C11		64.0	5.2	4.8
C12		73.1	4.8	4.8
C13		66.4	26.5	1.4
C14		68.8	28.9	2.9
C15		54.3	2.9	2.9
C16		51.6	1.4	1.4

5.6 Hobbs [74.1].

Specimen:

load path 1	$\sigma_1 > \sigma_2 = \sigma_3 > 0$	cylinder 55·110 mm.
load path 2	$0 < \sigma_1 < \sigma_2 = \sigma_3$	
load path 3	$\sigma_1 < 0 < \sigma_2 = \sigma_3$	cylinder 55·110 mm, waist: Ø = 49 – 53, length 64 mm.

Storage: Moist curing room until 7 days prior to testing.

Load path:
- path 1: Hydrostatic load, hereafter increasing σ_1 until failure.
- path 2: Hydrostatic load, hereafter decreasing σ_1 until failure.
- path 3: Proportional loading.

Load path 1

Number of Spec.	f_c MPa	σ_1 MPa	$\sigma_2 = \sigma_3$ MPa	age days
2	57.5	94.3	5.0	56
2		138.6	15.0	
2	41.4	69.1	5.0	
2		108.7	15.0	
2	30.2	55.9	5.0	
2		97.2	15.0	
2	18.7	41.5	5.0	
2		78.1	15.0	
2	46.9	79.4	5.0	14
2		124.0	15.0	
2	52.4	84.1	5.0	28
2		134.3	15.0	
3	54.9	91.3	5.0	56
3		139.8	15.0	
2	56.5	96.0	5.0	112
2		143.4	15.0	
2	33.9	58.9	5.0	14
2		104.3	15.0	
2	39.6	65.9	5.0	28
2		114.2	15.0	
3	43.4	69.8	5.0	56
3		116.5	15.0	
2	46.4	74.9	5.0	112
2		119.1	15.0	
2	22.5	48.4	5.0	14
2		94.9	15.0	
2	27.1	53.0	5.0	28
2		99.9	15.0	
3	31.8	58.4	5.0	56
3		102.9	15.0	
2	33.7	62.0	5.0	112
2		109.7	15.0	

Number of Spec.	f_c MPa	σ_1 MPa	$\sigma_2 = \sigma_3$ MPa	age days
2	15.0	42.2	5.0	14
2		89.2	15.0	
2	17.9	45.5	5.0	28
2		89.2	15.0	
3	22.0	47.9	5.0	56
3		90.7	15.0	
2	22.4	50.3	5.0	112
2		94.3	15.0	

Load path 2

Number of Spec.	f_c MPa	σ_1 MPa	$\sigma_2 = \sigma_3$ MPa	age days
1	30.2	0.0	31.8	56
1	18.7	0.7	23.4	56
2	22.5	0.0	24.4	14
2	27.1	0.2	28.2	28
3	31.8	0.1	30.3	56
2	33.7	0.5	36.0	112
2	15.0	0.2	19.5	14
2	17.9	0.1	19.0	28
3	22.0	0.4	25.0	56
2	22.4	0.4	26.7	112

Load path 3

Number of Spec.	f_c MPa	σ_1 MPa	$\sigma_2 = \sigma_3$ MPa	age days
3	57.5	-2.6	11.8	56
3		-2.4	25.4	
3	41.4	-2.6	12.0	
3		-2.0	20.0	
3		-0.8	30.0	
3	30.2	-2.2	10.1	
3		-1.8	17.8	
1		-0.6	19.0	
2	18.7	-1.8	8.2	
3		-1.3	10.5	
2		-0.8	11.7	

Number of Spec.	f_c MPa	σ_1 MPa	$\sigma_2 = \sigma_3$ MPa	age days
2	46.9	-2.7	7.5	14
2		-2.5	16.3	
2		-2.2	21.9	
2	52.4	-2.9	13.5	28
2		-2.5	16.2	
2		-2.3	21.5	
3	54.9	-2.9	13.6	56
3		-2.6	15.8	
3		-2.5	24.5	
2	56.5	-2.8	12.8	112
2		-3.1	20.5	
2		-2.4	23.7	
2	33.9	-2.2	10.0	14
2		-2.0	13.7	
2		-1.9	18.1	
2	39.6	-2.5	11.7	28
2		-2.7	15.9	
2		-2.1	20.4	
3	43.4	-2.8	12.0	56
3		-2.4	15.9	
3		-2.2	21.4	
2	46.4	-3.5	14.3	112
2		-2.9	17.2	
2		-2.2	22.0	
3	22.5	-1.9	9.0	14
1		-1.3	12.9	
1		-0.6	17.8	
2	27.1	-2.1	9.6	28
2		-1.5	14.6	
3	31.8	-2.3	10.4	56
3		-1.6	16.2	
3		-0.3	22.9	
2	33.7	-2.4	11.0	112
2		-1.6	16.7	
1		-0.4	23.2	
3	15.0	-1.4	6.7	14
2		-1.0	10.2	
2		-0.4	13.2	
2	17.9	-1.7	8.0	28
2		-1.1	9.6	
3	22.0	-1.9	8.6	56
3		-1.3	12.8	
3		-0.6	16.4	
2	22.4	-2.1	9.7	112
2		-1.4	14.4	

5.7 Bremer and Steinsdörfer [76.1].

Specimen: 100 mm cubes.

Storage: 7 days in water, 100 days in air.

Load Path: Proportional loading.

1/ $\sigma_1 \geq \sigma_2 \geq \sigma_3 \geq 0$

2/ $\sigma_1 \geq \sigma_2 \geq 0 \geq \sigma_3$

V_{aggr}: 0.6 – 0.7.

Special: Friction between load platens and concrete was reduced by two layers of aluminum foil with grease in between.

The test rig used was a one–part machine where the jacks are in a fixed position at all times during the test.

Load path 1

Number of spec.	f_c MPa	σ_1 MPa	σ_2 MPa	σ_3 MPa
6	42.8	65.4	65.4	1.3
		66.3	33.1	1.3
		63.3	31.7	1.3
	43.6	64.6	64.6	1.3
		65.0	32.6	1.3
		62.4	31.2	1.3
	53.7	78.0	78.0	1.1
		84.9	59.4	1.2
		83.3	58.3	0.8
		75.8	37.9	1.1
		67.2	6.7	1.0
	53.0	76.8	76.8	1.6
		74.6	74.6	0.9
		81.0	68.8	1.2
		78.4	66.6	1.1
		75.7	37.9	1.5
		72.6	36.3	1.0
		69.9	35.0	0.5
		67.2	20.1	1.0
		64.0	19.2	0.5
		61.4	6.2	1.3
		56.7	5.7	0.8
	63.4	87.4	87.4	1.8
		89.3	44.6	1.8
		81.1	40.6	1.2
	63.1	83.8	83.8	1.7
		86.4	43.1	1.8
		78.2	39.1	1.1

Load path 2

Number of spec.	f_c MPa	σ_1 MPa	σ_2 MPa	σ_3 MPa
6	42.8	19.6	19.6	-2.0
		45.0	45.0	-0.9
		36.9	18.4	-1.2
		25.4	7.6	-2.5
	43.6	43,4	43.4	-0.9
		38.0	19.0	-1.2
		42.7	4.3	-0.5
	53.7	56.9	56.9	-1.2
		37.3	26.1	-2.3
		39.2	27.5	-1.5
		39.7	19.7	-2.4
		52.0	5.2	-0.5
	53.0	27.5	27.5	-2.7
		53.0	53.0	-1.1
		57.4	57.4	-0.6
		29.4	25.0	-1.8
		43.6	37.1	-0.9
		33.0	21.0	-2.0
		42.9	27.9	-0.9
		32.9	16.4	-2.0
		39.2	19.6	-1.2
		28.3	8.5	-2.7
		40.7	12.2	-0.8
		49.0	4.9	-0.5
	63.4	28.5	28.5	-2.8
		63.7	63.7	-1.3
		44.6	21.8	-1.4
	63.1	60.5	60.5	-1.2
		66.2	66.2	-0.7

5.8 Linse and Aschl [76.2].

Specimen: 100 mm cubes.

Storage: 7 days in moist condition, hereafter in sealed plastic bags for 130 days.

Load Path: 1/ Hydrostatic load, hereafter increasing σ_1.
2/ Proportional load path.
3/ Hydrostatic load, hereafter increasing σ_2 and σ_3.

V_{aggr}: 0.6 – 0.7.

Special: Friction restraint reduced by using brush–platens.

The test rig used was a one–part machine where the jacks are in a fixed position at all times during the test.

Load path 1

Spec. no.	f_c MPa	σ_1 MPa	σ_2 MPa	σ_3 MPa
13	34.4	64.5	6.5	6.5
15		119.5	26.5	26.5

Load path 2

Spec. no.	f_c MPa	σ_1 MPa	σ_2 MPa	σ_3 MPa
11	34.4	99.0	13.9	13.9
12		82.0	9.8	9.8
16		137.5	26.1	26.1
21	36.0	93.0	93.0	18.6
22		66.2	6.6	6.6
24		61.2	5.5	5.5
42	35.2	80.5	9.7	9.7
43		142.5	72.7	18.5
44		94.5	51.0	8.5
45		66.0	6.6	6.6
46		67.5	6.8	4.0
51	33.1	94.0	20.7	10.3
52		93.0	87.4	20.5
53		100.0	20.0	20.0
72	36.1	93.2	45.2	8.3
73		102.9	50.9	7.7
74		73.2	7.3	7.2
75		64.3	5.8	4.1
76		64.9	6.6	4.3

Spec. no.	f_c MPa	σ_1 MPa	σ_2 MPa	σ_3 MPa
81	35.2	54.2	4.0	3.5
82		87.7	20.6	8.3
83		98.0	25.4	9.4
84		71.4	35.3	4.0
85		73.2	18.9	6.0

Load path 3

Spec. no.	f_c MPa	σ_1 MPa	σ_2 MPa	σ_3 MPa
23	36.0	25.0	96.2	96.2
25		15.0	81.0	81.0
26		10.5	84.0	84.0

5.9 Rossi [76.3].

Specimen: Load path 1 – 3: 100 mm cubes, load path 4: cylinders 160·320 mm.

Storage: 7 days in fog room, hereafter more than 120 days in plastic bags.

Load Path: Hydrostatic load up to specified level, hereafter:

1/ $\Delta\sigma_1 = -\frac{1}{2}\Delta\sigma_2 = -\frac{1}{2}\Delta\sigma_3$

2/ $\Delta\sigma_1 = -\Delta\sigma_3$, $\Delta\sigma_2 = 0$

3/ $\Delta\sigma_1 = \Delta\sigma_2 > 0$, $\Delta\sigma_3 = -2\Delta\sigma_1$

4/ Decreasing σ_1 to failure $\sigma_1 \leq 0$ at failure.

V_{aggr}: > 0.6.

Special: Friction was reduced by using four polyethylene sheets with MO_2S–grease in between (approx. 0.25 mm thickness).

The test rig used for load paths 1 – 3 was a one–part machine where the jacks are in a fixed position at all times during the test.

Load path 1

Spec. no.	f_c MPa	σ_1 MPa	$\sigma_2 = \sigma_3$ MPa
T1-1	26.7	37.2	1.4
T2-4		36.7	1.7
T4-1		36.6	1.7
T6-1		35.6	2.2
T1-4		50.8	4.2
T3-1		50.1	4.6
T4-4		51.0	4.1
T6-2		48.1	5.6
T2-1		64.2	7.9
T3-4		64.1	7.9
T5-1		62.8	8.5
T7-1		64.7	7.7
T1-2		78.8	10.9
T2-5		77.1	11.7
T4-2		79.2	10.5
T8-1		77.3	11.6
T5-4		88.5	15.8
T6-4		87.5	16.2
T7-4		89.0	15.6
T9-1		92.6	13.8

Load path 2

Spec. no.	f_c MPa	σ_1 MPa	σ_2 MPa	σ_3 MPa
T1-5	26.7	39.4	0.1	19.8
T3-2		39.5	0.1	19.7
T4-5		39.7	0.1	19.7
T6-3		39.0	0.7	19.8
T2-2		50.5	2.7	26.8
T3-5		50.8	2.4	26.7
T5-2		50.2	2.8	26.8
T7-2		50.9	2.1	26.8
T1-3		62.7	4.3	33.4
T2-6		62.7	4.3	33.4
T4-3		63.4	3.6	33.4
T8-2		62.1	4.7	33.4
T5-5		72.5	7.8	40.0
T6-5		71.8	8.5	40.1
T7-5		73.1	7.4	40.1
T9-2		74.9	5.5	40.1

Load path 3

Spec. no.	f_c MPa	σ_1 MPa	$\sigma_2 = \sigma_3$ MPa
T2-3	26.7	1.3	39.6
T3-6		1.7	39.3
T5-3		1.8	39.2
T7-3		1.2	39.5
T1-6		3.2	48.5
T3-3		2.9	48.7
T4-6		3.2	48.5
T8-3		2.4	49.0
T5-6		5.4	57.5
T6-6		4.9	57.7
T7-6		5.2	57.4
T9-3		3.1	58.7
T8-6		38.4	0.8
T9-4		38.2	0.8
T9-4b		37.1	1.4
T8-5		63.6	8.0
T8-5b		63.6	8.0
T9-6b		64.7	7.5
T8-6b		87.7	15.4
T9-5		90.6	14.3
T9-5b		89.4	14.8

Load path 4

Spec. no.	f_c MPa	σ_1 MPa	$\sigma_2 = \sigma_3$ MPa
T5-2	28.4	-3.1	0.0
T6-2		-2.0	0.0
T7-2		-2.9	0.0
T8-2		-2.2	0.0
T5-3		-2.5	6.3
T6-3		-2.3	6.3
T7-3		-2.5	6.3
T8-3		-2.5	6.3
T5-4		-2.5	12.2
T6-4		-2.1	12.2
T7-4		-2.4	12.2
T8-4		-2.5	12.2
T5-5		-2.0	18.0
T6-5		-1.7	18.0
T7-5		-1.5	18.0
T8-5		-1.8	18.0
T5-6		-1.1	23.9
T6-6		-1.3	23.9
T7-6		-1.3	23.9
T8-6		-0.9	23.9

5.10 Schickert and Winkler [77.4].

Specimen: 100 mm cubes.

Storage: 7 days in fog room, hereafter more than 200 days in plastic bags.

Load Path: Hydrostatic load up to specified level, hereafter:

1/ $\Delta\sigma_1 = -\frac{1}{2}\Delta\sigma_2 = -\frac{1}{2}\Delta\sigma_3$

2/ $\Delta\sigma_1 = -\Delta\sigma_3$, $\Delta\sigma_2 = 0$

3/ $\Delta\sigma_1 = \Delta\sigma_2 > 0$, $\Delta\sigma_3 = -2\Delta\sigma_1$

4/ Proportional load path.

V_{aggr}: > 0.6.

Special: Friction was reduced by using flexible load platens.
The test rig used was a one–part machine where the jacks are in a fixed position at all times during the test.

Deformations were measured using strain gauges mounted in groves in some of the specimens. These specimens showed less increase in strength compared to specimens without gauges.

Load path 1

Spec. no.	f_c MPa	σ_1 MPa	σ_2 MPa	σ_3 MPa	gauge
1a-4	33.4	62.5	7.0	7.2	Y
3a-1	32.1	60.6	7.9	8.1	Y
4a-4	34.5	59.2	8.4	8.6	Y
6a-1	33.3	63.2	6.5	6.9	
9a-1	38.5	65.0	5.9	5.9	
2a-1	34.7	75.2	13.3	13.1	Y
3a-4	32.1	75.6	14.2	14.0	Y
5a-1	32.9	74.0	14.5	14.6	Y
6a-4	33.3	81.0	11.0	11.1	
8a-1	37.7	85.2	9.4	9.4	
9a-4	38.5	82.5	9.8	9.8	
1a-1	33.4	85.6	22.4	22.0	Y
2a-4	34.7	97.5	15.3	15.2	Y
4a-1	34.5	94.6	15.9	15.9	Y
5a-4	32.9	94.9	16.4	16.2	
7a-1	37.7	88.2	19.6	19.7	
8a-4	37.7	100.0	13.4	13.3	
1a-2	33.4	106.0	23.5	23.5	Y
2a-5	34.7	109.6	21.5	20.5	Y
5a-5	32.9	101.0	25.6	26.3	
7a-2	37.7	112.4	20.0	20.0	
8a-5	37.7	112.1	20.4	21.0	

Load path 2

Spec. no.	f_c MPa	σ_1 MPa	σ_2 MPa	σ_3 MPa	gauge
1a-3	33.4	78.9	42.6	6.4	Y
2a-6	34.7	79.0	42.7	6.3	Y
4a-3	34.5	81.6	42.8	4.7	Y
5a-6	32.9	77.9	42.7	7.5	
7a-3	37.7	79.5	44.4	6.3	
8a-6	37.7	84.7	45.4	4.6	
2a-3	34.7	93.7	51.6	8.2	Y
3a-6	32.1	93.1	51.1	9.2	Y
5a-3	32.9	93.0	51.6	10.3	Y
6a-6	33.3	93.8	51.1	8.4	
8a-3	37.7	95.3	51.7	7.4	
9a-6	38.5	93.5	51.1	8.1	

Load path 3

Spec. no.	f_c MPa	σ_1 MPa	σ_2 MPa	σ_3 MPa	gauge
3a-2	32.1	61.9	61.6	3.8	Y
4a-5	34.5	61.8	61.8	3.8	Y
6a-2	33.3	61.7	61.8	3.1	
3a-5	32.1	59.8	60.1	5.8	Y
1a-6	33.4	73.5	73.4	5.7	Y
3a-3	32.1	73.0	73.2	7.2	Y
4a-6	34.5	73.3	73.4	6.0	Y
6a-3	33.3	73.4	73.1	5.6	
9a-3	38.5	74.3	73.8	4.5	

Load path 4

Spec. no.	f_c MPa	σ_1 MPa	σ_2 MPa	σ_3 MPa	gauge
5a-2	32.9	60.1	6.2	6.3	
5a-6	32.9	60.0	6.0	6.0	
7a-3	37.7	69.1	6.9	6.9	
8a-6	37.7	70.8	7.1	7.1	
2a-6	34.7	120.1	24.6	24.6	
4a-3	34.5	116.2	23.8	23.6	
9a-2	38.5	104.0	21.2	21.1	
2a-2	34.7	94.2	50.1	6.8	
2a-3	34.7	87.2	46.6	6.5	
3a-6	32.1	91.9	49.0	6.6	
5a-3	32.9	69.8	37.3	5.0	Y
2a-2	34.7	59.5	58.7	3.0	Y
3a-5	32.1	65.5	65.1	3.2	
5a-2	32.9	57.3	57.0	2.8	
6a-5	33.3	67.6	66.1	3.3	
8a-2	37.7	66.6	65.5	3.0	
9a-5	38.5	71.8	71.1	3.3	

Spec. no.	f_c MPa	σ_1 MPa	σ_2 MPa	σ_3 MPa	gauge
9a-2	38.5	91.5	91.6	7.5	
1a-6	33.4	73.7	73.6	6.1	Y
3a-3	32.1	75.1	75.1	6.3	
4a-6	34.5	79.8	79.8	6.5	

5.11 Bellotti and Ronzoni [84.1].

Specimen: Cylinder 160·320 mm.

Storage: ?.

Load Path: Hydrostatic load up to specified level, hereafter increasing σ_1 until failure.

V_{aggr}: ?.

Number of spec.	f_c MPa	σ_1 MPa	$\sigma_2 = \sigma_3$ MPa
8	55.7	85.8	4.9
8		109.8	9.8
8		129.5	14.7
8		147.3	19.6
7		165.4	24.5
8		182.0	29.4
8		199.1	34.3

5.12 Jan G.M. van Mier [84.12].

Specimen: 100 mm cubes.
Storage: Stored in water for 28 days, hereafter sealed in bags for 42 days.
Load Path: Proportional load path.
V_{aggr}: ?.
Special: Friction reduced by using brush platens instead of solid load platens.

The specimens were tested in a 4–part machine.

Spec. no.	f_c MPa	σ_1 MPa	σ_2 MPa	σ_3 MPa
8A1-3	45.3	82.9	28.0	4.6
8B1-1		73.0	22.4	4.1
8B2-2		106.3	18.8	10.9
8B2-3		111.3	67.1	11.4
8B2-5		85.6	28.7	4.6
8A2-5		84.8	8.9	9.0
9A1-5	47.9	12.2	-1.9	1.6
9A2-4		67.1	6.7	3.9
9A2-5		127.0	42.0	13.3
9B2-2		96.9	62.3	5.2
9B2-3		116.9	49.1	11.8
9B2-4		121.1	33.1	12.2
9B2-5		85.1	13.1	4.6

5.13 Winkler [85.2].

Specimen: 100 mm cubes.
Storage: 7 days in water.
Load Path: Proportional load path.
V_{aggr}: > 0.7.
Special: Friction reduced by using brush platens instead of solid load platens.

The specimens were tested, partly in a 1–part machine, and partly in a multi–part machine.

Spec. no.	f_c MPa	σ_1 MPa	$\sigma_2 = \sigma_3$ MPa	machine (part)
1	20.7	49.6	2.5	one
2		54.2	2.7	
3		54.2	2.7	
4		53.5	2.7	
5		57.3	2.9	
6		53.9	2.7	
7		51.3	2.6	
8		54.7	2.7	multi
9		51.2	2.6	
10		57.5	2.9	
11		56.2	2.8	
12		57.6	2.9	
13		53.0	2.7	
14		51.2	2.6	
15		50.5	2.5	
16		50.3	2.5	
17		52.0	2.6	
18		53.6	2.7	
19		49.9	2.5	
20		51.1	2.6	
21		45.7	2.3	
22		46.1	2.3	
23		50.6	2.5	

5.14 Chuan–zhi, Zhen–hai and Xiu–qin [87.1].

Specimen: 100 mm cubes.
Storage: 28 days in fog room.
Load Path: Proportional load path.
V_{aggr}: ?.
Special: Friction reduced by using two teflon sheets with MO_2S–grease in between.

The test rig used was a one–part machine where the jacks are in a fixed position at all times during the test.

Spec. no.	f_c MPa	σ_1 MPa	σ_2 MPa	σ_3 MPa
1-2	9.4	37.0	3.9	3.9
3-3		29.8	3.9	3.0
6-2		45.3	8.5	4.4
2-2		46.6	14.3	5.7
1-3		46.1	18.8	4.6
6-3		43.2	17.1	4.2
2-3		52.9	26.6	5.0
5-2		75.0	15.2	15.7
7-2		58.1	11.5	12.4
7-3		67.3	14.1	14.8
4-3		96.1	28.6	29.0
3-2		96.1	29.2	29.4
40-2	10.7	45.2	9.4	5.0
41-2		49.0	14.3	4.9
40-3		47.6	23.9	4.7
41-3		48.0	36.0	4.7
45-2		43.2	32.6	4.2
46-3		38.4	34.1	3.9
45-3		38.4	37.1	3.7
46-2		38.4	38.4	3.7
42-2		91.3	27.4	18.5
43-2		86.0	25.9	17.5
42-3		86.5	34.9	18.0
44-2		91.3	36.5	18.3
43-3		84.6	43.0	17.8
44-3		91.3	45.1	18.4

BIBLIOGRAPHY

[28.1] *A Study of the Failure of Concrete Under Combined Compressive Stresses.*
F.E. Richart, A. Brandtzaeg, and R.L. Brown, Bulletin no. 185,
Engineering Experiment Station, University of Illinios, Urbana 1928.

[52.1] *A General Analytical Solution for Mohr's Envelope*
G. Balmer, ASTM Proceedings, 1952, pp 1260 – 1271

[56.1] *Proposed International Methods of Tensting Concretes.*
RILEM bulletin no. 33, 1956, pp 71 – 73

[57.1] *Lightweight–Aggregate Concrete for Structural Use.*
J.J. Shideler, Journal of the ACI, Oct. 1957, pp 299 – 328.

[60.1] *Betongens trykkfasthet – terning eller sylinder?*
H. Hansen, A. Kielland, K.E.C. Nielsen, and S. Thaulow,
Nordisk Beton, 1960, 4, pp 305 – 324, or
RILEM, Bulletin no. 17, Dec. 1962, pp 23 – 34.

[60.2] *Researches Toward a General Flexural Theory for Structural Concrete.*
H. Rüsch, Journal of the ACI, Jul 1960, pp 1 – 26.

[61.1] *Strength of Concrete Under Combined Stress.*
C.J. Bellamy, Journal of the ACI, Oct. 1961, pp 367 – 381.

[61.2] *Concrete under triaxial stress.*
T.N.W. Akroyd, Magazine of Concrete Research, vol. 13, no. 39, Nov. 1961,
pp 111 – 118.

[63.1] *Strength of Structural Lightweight Concrete Under Combined Stress.*
J.K.A. Hanson, Portland Cement Association, Journal of the Research and
Developement Laboratories, vol. 1, 1963, pp 39 – 46.

[63.2] *Variables in Concrete Aggregates and Portland Cement Past which Influence the Strength of Concrete.*
W.A. Cordon and H.A. Gillespie, Journal of the ACI, Aug. 1963,
pp 1029 – 1051.

[64.1] *The Testing of Brittle Materials Under Uniform Uniaxial Compressive Stresses.*
K. Newman and L. Lahance, ASTM proceedings, vol. 64, 1964, pp 1044 – 1067.

[65.1] *Kritische Spannungszustände des Betons bei mehrachsiger, ruhender Kurzzeitbelastung.*
H. Reimann, Deutscher Ausschuss für Stahlbeton, Heft 175, Berlin 1965.

[69.1] *Triaxial Behavior of Concrete*
N.J. Gardner, Journal of the ACI, Feb. 1969, pp 136 – 146.

[69.2] *The influence of aggregate particles on the local strain distribution and fracture mechanism of cement paste during drying shrinkage and loading to failure.*
D.R. McCreath, J.B. Newman, and K. Newman. Materials and Structures,
RILEM, no. 7, Jan. 1969, pp 73 – 84.

[70.1] *Strength and Deformation Properties of Plain Concrete Subject to Combined Stress. Part 1: Strength Results Obtained on one Concrete.*
D.W. Hobbs, Cement and Concrete Association, report 42.451, Nov. 1970.

[70.2] *Compressive Strength of Plain Concrete Under Multiaxial Loading Conditions.*
L.L. Mills and R.M. Zimmerman, Journal of the ACI, Oct. 1970, pp 802 – 806.

[71.1] *General Behavior Theory for Cement Pastes, Mortars, and Concretes.*
M.A. Taylor, Journal of the ACI, Oct. 1971, pp 756 – 762.

[72.1] *Strain and Ultimate Strength of Concrete Under Triaxial Stress.*
P. Launay and H. Gachon, ACI SP–34, 1972, pp 269 – 281.

[72.2] *On a Triaxial Strength Criterium for Concrete.*
F. Bremer, ACI SP–34, 1972, pp 283 – 294.

[72.3] *Concrete Strength in Multiaxial Stress States.*
V. Hansson and K. Schimmelpfennig, ACI SP–34, 1972, pp 295 – 311,

[72.4] *Strength and Deformation Properties of Plain Concrete Subject to Combined Stress. Part 2: Strength in Multiaxial Compression.*
D.W. Hobbs, Cement and Concrete Association, report 42.463, Nov. 1972.

[72.5] *Experimental Research an Deformation and Failure of Concrete Under Triaxial Loads.*
P. Bertacchi and R. Bellotti, The Deformations and Rupture of Solids Subjected to Multiaxial Stresses, RILEM internat. symposium, Cannes 1972.

[72.6] *The Strength and Deformation Properties of Plain Concrete Under Combined Stress.*
D.W. Hobbs, The Deformations and Rupture of Solids Subjected to Multiaxial Stresses, RILEM internat. symposium, Cannes 1972.

[72.7] *The Measurement and Estimation of the Strain in Concrete Under Multiaxial Stress.*
J.M. Illston, I.J. Jordan, and L.J.Parrott, The Deformations and Rupture of Solids Subjected to Multiaxial Stresses, RILEM internat. symposium, Cannes 1972.

[72.8] *Fracture Criteria of Cement Paste, Mortar, and Concrete Subjected to Multiaxial Compressive Stresses.*
S. Kobayashia and Koyanagi, The Deformations and Rupture of Solids Subjected to Multiaxial Stresses, RILEM internat. symposium, Cannes 1972.

[72.9] *The Cracking and Failure of Concrete Under Combined Stresses and its Implications for Structural Design.*
J.B. Newman and K. Newman, The Deformations and Rupture of Solids Subjected to Multiaxial Stresses, RILEM internat. symposium. Cannes 1972.

[72.10] *Major Factors Affecting the Multiaxial Compressive Strength of Plain Concrete.*
M. Zimmerman, The Deformations and Rupture of Solids Subjected to Multiaxial Stresses, RILEM internat. symposium, Cannes 1972.

[73.1] *The Strength and Deformation of Concrete under Short–Term Loading – A Review.*
D.W. Hobbs, Cement and Concrete Association, report 42.484, Sep. 1973.

[73.2] *Versuchsanlage zur Ermittlung der Dreiachsigen Festigkeit von Beton mit Ersten Versuchsergebnissen.*
D. Linse, Cement and Concrete Research, vol. 3, no. 4, 1973, pp 445 – 457.

[73.3] *Comportemento del Calcestruzzo Sottoposto a Sollecitazioni Pluriasiali: Indagini Sperimentali per la Determinazione Della Superficie di Rottura (Failure Surface).*
R. Bellotti and P. Rossi, ENEL internal report 2322, Italy, Mar. 1973.

[73.4] *Comportemento del Calcestruzzo Sottoposto a Sollecitazioni Pluriasiali: Indagini Sperimentali per la Determinazione Degli Stati Fisci del Calcestruzzo Precedenti alla Rottura.*
R. Bellotti and P. Rossi, ENEL internal report 2352, Italy, Apr. 1973.

[74.1] *Strength and Deformation Properties of Plain Concrete Subject to Combined Stress. Part 3: Results Obtained on a Range of Flint Gravel Aggregate Concretes.*
D.W. Hobbs, Cement and Concrete Association, report 42.497, Jul. 1974.

[74.2] *Nomograms for the Failure of Plain Concrete Subjected to Short Term Multiaxial Stresses.*
D.J. Hannant, The Structural Engineer, vol. 52, no. 5, May 1974.

[74.3] *Apparatus for testing concrete under multiaxial states of stress.*
J.B. Newman, Magazine of Concrete Research, vol. 26, no. 89, Dec. 1974.

[74.4] *New Prospects for Evaluating the Degree of Safety in Concrete Structures Subjected to Multiaxial Stresses.*
R. Bellotti and P. Rossi, ENEL internal report 2458, Italy, Oct. 1974.

[76.1] *Bruchfestigkeiten und Bruchverformung von Beton unter mehraxialer Belastung bei Raumtemperatur.*
F. Bremer and F. Steinsdörfer, Deutscher Ausshuss für Stahlbeton, Heft 263, Berlin 1976.

[76.2] *Versuche zum Verhalten von Beton unter mehrachsiger Beanspruchung.*
S. Stöckl and E. Grasser, Technische Universität München, internal report, May 1976.

[76.3] *Cooperative Research on Properties of Concrete, ENEL–CRIS Test Results.*
P. Rossi, ENEL preliminary report 2590, Italy, Mar. 1976.

[77.1] *Triaxial Stress–Strain Relationship for Concrete.*
L. Cedolin, Y.R.J. Crutzen, and S. Dei Poli, Journal of the Eng. Mech. Div. ASCE, EM3, Jun 1977, pp 423 – 439.

[77.2] *Behavior of Concrete Under Multiaxial Stress.*
M.D. Kotsovos and J.B. Newman, Journal of the ACI, Sep. 1977, pp 443 – 446.

[77.3] *Design stresses for concrete structures subject to multi–axial stresses.*
D.W. Hobbs, C.D. Pomeroy, J.B. Newman, The Structural Engineer, vol. 55, no. 4, Apr 1977, pp 151 – 164.

[77.4] *Results of tests Concerning Strength and Strain of Concrete Subjected to multiaxial Compressive Stresses.*
Schickert and Winkler, Deutscher Ausschuss für Stahlbeton, Heft 277, Berlin 1977.

[77.5] *Mekanik 2.2 del 2, 2'nd edition.*
M.P. Nielsen, L. P. Hansen, and A. Rathkjen, ABK, DTH (published as manuscript), Denmark, 1977.

[77.6] *A Failure Criterion for Concrete.*
N.S. Ottosen, Journ. of the Eng. Mech. Div. ASCE, EM4, Aug. 1977, pp 527 – 535.

[78.1] *Generalized Stress–Strain Relations for Concrete.*
M.D. Kotsovos and J.B. Newman, Journ. of the Eng. Mech. Div. ASCE, EM4, Aug. 1978, pp 845 – 856.

[78.2] *Strength of Concrete under Multiaxial Stress States.*
K.H. Gerstle et.al., ACI SP–55, 1978, pp 103 – 131.

[78.3] *Lösung versuchtechnischer Fragen bei der Emittlung des Festigkeits– und Verformungsverhaltens von Beton unter dreiachsiger Belastung.*
D. Linse, Deutscher Ausschuss für Stahlbeton, Heft 292, Berlin 1978.

[79.1] *A mathematical description of the deformational behavior of concrete under complex loading.*
M.D. Kotsovos and J.B. Newman, Magazine of Concrete Research, vol. 31, no. 107, Jun. 1979, pp 77 – 90.

[79.2] *Constitutive Model for Short–Time Loading of Concrete.*
N.S. Ottosen, Journ. of the Eng. Mech. Div. ASCE, EM1, Feb. 1979, pp 127 – 141.

[79.3] *A mathematical description of the strength properties of concrete under generalized stress.*
M.D. Kotsovos, Magazine of Concrete research, vol. 31, no. 108, Sep. 1979, pp 151 – 158.

[79.4] *Effect of Stress Path on the Behavior of Concrete Under Triaxial Stress States.*
M.D. Kotsovos, Journal of the ACI, Feb. 1979, pp 213 – 223.

[80.1] *Behavior of Concrete under Multiaxial Stress States.*
K.H. Gerstle et.al., Journ. of the Eng. Mech. Div. ASCE, EM6, Dec. 1980, pp 1383 – 1403.

[80.2] *Total Strain Theory and Path–Dependence of Concrete.*
Z.P. Bazant and T. Tsubaki, Journ. of the Eng. Mech. Div. ASCE, EM6, Dec. 1980, pp 1151 – 1173.

[80.3] *Constitutive Models for Concrete Structures.*
W.F. Chen and E.C. Ting, Journ. of the Eng. Mech. Div. ASCE, EM1, Feb. 1980, pp 1 – 19.

[81.1] *Simple Formulation of Triaxial Concrete Behavior.*
K.H. Gerstle, Journal of the ACI, Sep. 1981, pp 382 – 387.

[81.1] *Failure Criteria for Concrete.*
D.W. Hobbs, Manuscript to be published by Pitman Books Ltd in 'Handbook of Structural Concrete'. Manuscript dated Sep. 1981.

[81.3] *The influence of pore pressure upon concrete.*
J.E. Butler, Magazine of Concrete Research, vol. 33, no. 114, Mar. 1981, pp 3 – 17.

[82.1] *Complete Triaxial Stress–Strain Curves for Concrete.*
S.H. Ahmad and S.P. Shah, Journ. of the Struc. Div. ASCE, ST4, Apr. 1982, pp 728 – 742.

[82.2] *Constitutive relations and a failure criterion for concrete based on fundamental material properties.*
P. Montague and K.Kormi, Magazine of Concrete Research, vol. 34, no. 118, Mar. 1982, pp 35 – 43.

[82.3] *Plasticity in Reinforced Concrete.*
W.F. Chen, McGraw–Hill Book Company, New York 1982.

[83.1] *Building Code Requirements for Reinforced Concrete (ACI 318 – 83).*
American Concrete Institute, Detroit, Michigan, 1983.

[84.1] *Results of Tests Carried out on Cylindrical Concrete Specimens Subjected to Complex Stress States: A Critical Analysis.*
R. Bellotti and E. Ronzoni, Int. Conf. on Concrete under Multiax. Cond., RILEM, Press de l'Universite Paul Sabatier, Toulouse, May 1984, pp 53 – 74.

[84.2] *Fundamental Investigations on the Influence of Test Equipment on Multiaxial Test Results of Concrete.*
H. Winkler, Int. Conf. on Concrete under Multiax. Cond., RILEM, Press de l'Universite Paul Sabatier, Toulouse, May 1984, pp 9 – 19.

[84.3] *Complete Stress–Strain Behavior and Damaging Status of Concrete under Multiaxial Conditions.*
J.G.M. van Mier, Int. Conf. on Concrete under Multiax. Cond., RILEM, Press de l'Universite Paul Sabatier, Toulouse, May 1984, pp 75 – 85.

[84.4] *Simple Formulation of Concrete Behavior under Triaxial Load Cycles.*
R. Scavuzzo, K.H. Gerstle, and H.Y. Ko, Int. Conf. on Concrete under Multiax. Cond., RILEM, Press de l'Universite Paul Sabatier, Toulouse, May 1984, pp 114 – 123.

[84.5] *Behavior of Concrete under Multiaxial Load Histories.*
T. Stankowski and K.H. Gerstle, Int. Conf. on Concrete under Multiax. Cond., RILEM, Press de l'Universite Paul Sabatier, Toulouse, May 1984, pp 124 – 132.

[84.5] *Failure Envelope of Concrete Subjected to Multiaxial Compressive Stresses.*
Y. Nojiri, K. Kotani, and Y. Abe, Int. Conf. on Concrete under Multiax. Cond., RILEM, Press de l'Universite Paul Sabatier, Toulouse, May 1984, pp 141 – 148.

[84.7] *Triaxial Behavior of Concretes of Different Weights.*
M. Berra, A. Fatticcioni, and G. Ferrara, ENEL internal report 3166, 1984.

[84.8] *Orthotropic Model for Complete Stress–Strain Curves of Concrete under Multiaxial Stresses.*
S.H. Ahmad, S.P. Shah, Int. Conf. on Concrete under Multiax. Cond., RILEM, Press de l'Universite Paul Sabatier, Toulouse, May 1984, pp 251 – 262.

[84.9] *Testing Methods.*
G. Schickert, Int. Conf. on Concrete under Multiax. Cond. vol II, RILEM, Press de l'Universite Paul Sabatier, Toulouse, May 1984, pp 10 – 19.

[84.10] *Parameters for Constitutive Modeling.*
S.P. Shah, Int. Conf. on Concrete under Multiax. Cond. vol II, RILEM, Press de l'Universite Paul Sabatier, Toulouse, May 1984, pp 33 – 67.

[84.11] *Considerations on International comparative Investigations on Concrete Subjected to Multiaxial Compressive Stresses.*
G. Schickert and H. Winkler, Int. Conf. on Concrete under Multiax. Cond. vol II, RILEM, Press de l'Universite Paul Sabatier, Toulouse, May 1984, pp 85 – 96.

[84.12] *Strain–Softening of Concrete under Multiaxial Loading Conditions.*
J.G.M. van Mier, Doctoral thesis, Eindhoven, Holland, 1984.

[84.13] *Limit Analysis and Concrete Plasticity.*
M.P. Nielsen, Prentice–Hall, Englewood Cliffs, New Jersey, 1984.

[84.14] *DS 423.23 Betonprøvning. Hærdnet beton. Trykstyrke. 2. udg.*
Dansk Standart, 1984.

[85.1] *Simple Formulation of Concrete Behavior Under Multiaxial Load Histories.*
T. Stankowski and K.H. Gerstle, Journal of the ACI, Mar 1985, pp 213 – 221.

[85.2] *Grundsätzliche Untersuchungen zum Geräteeinfluss bei der mehraxialen Druckprüfung von Beton.*
H. Winkler, Deutscher Ausschuss für Stahlbeton, Heft 366, Berlin 1985.

[85.3] *Influence of Damage Orientation Distribution on the Multiaxial Stress Strein Behavior of Concrete.*
J.G.M. van Mier, Cement and Concrete Research, vol. 15, 1985, pp 849 – 862.

[86.1] *Orthotropic Model of Concrete for Triaxial Stresses.*
S.H. Ahmad, A.R. Khaloo, Journ. of Struc. Eng. ASCE, vol. 112, no. 1, Jan. 1986, pp 165 – 181.

[86.2] *Large triaxial–torsional testing machine with hygrothermal control.*
Z. Bazant, R. Vaitys, R. Klima, and J.D. Hess, Materials and Structures, RILEM, no. 112, Jul. 1986, pp 285 – 294.

[86.3] *Fracture of Concrete under Complex Stress.*
J.G.M. van Mier, HERON, vol. 31, no. 3, 1986.

[86.4] *Advanced Triaxial Testing of Soil and Rock.*
ed. Donaghe, Chaney, and Silver, ASTM STP 977, 1986.

[87.1] *Experimental Investigation of Biaxial and Triaxial Compressive Concrete Strength.*
W. Chuan–zi, G. Zhen–hai, and Z. Xiu–qin, ACI Materials Journal, Mar. 1987, pp 92 – 100.

[87.2] *Properties of Concrete, 3'rd edition.*
A.M. Neville, Longman Scientific & Technical, England 1987.

[88.1] ***Højstyrkebetons Deformationsforhold.***
M.B. Sørensen, M.Sc. thesis, ABK/LBM, DTH, Denmark, 1988.

[88.2] ***Behavior of High–Strength Concrete under Torsional Triaxial Compression.***
A.R. Khaloo and S.H. Ahmad, ACI Materials Journal, Nov. 1989, pp 550 – 558.

[89.1] ***Concrete over the Top, or: Is There Life after Peak?***
S.S. Smith, K.J. Willam, K.H. Gerstle, and S. Sture, ACI Materials Journal, Sep. 1989, pp 491 – 497.

[89.2] ***Review of Constitutive Models for Concrete.***
Y. Xiaoquin, N.S. Ottosen, S. Thelandersson, M.P. Nielsen, Report to the Commision of the European Comunities Joint Research Centre ISPRA, 1989.

AFDELINGEN FOR BÆRENDE KONSTRUKTIONER
DANMARKS TEKNISKE HØJSKOLE

Department of Structural Engineering
Technical University of Denmark, DK–2800 Lyngby

SERIE R
(Tidligere: Rapporter)

R 230. RIBERHOLT, H.: Woodflanges under tension, 1988.
R 231. HOLKMANN OLSEN, N.: Implementation. 1988. (public. pending).
R 232. HOLKMANN OLSEN, N.: Uniaxial. 1988. (public pending)
R 233. HOLKMANN OLSEN, N.: Anchorage. 1988. (public pending)
R 234. HOLKMANN OLSEN, N.: Heat Induced. 1988. (public pending)
R 235. SCHEEL, HELLE: Rotationskapacitet. 1988. (public pending)
R 236. NIELSEN, MONA: Arbejdslinier. 1988. (public pending)
R 237. GANWEI, CHEN: Plastic Analysis of Shear in Beams. Deep Beams and Corbels. 1988.
R 238. ANDREASEN, BENT STEEN: Anchorage of Deformed Reinforcing bars. 1988.
R 239. ANDREASEN, BENT STEEN: Anchorage Tests with deformed Reinforcing Bars in more than one layer at a Beam Support. 1988.
R 240. GIMSING, N.J.: Cable–Stayed Bridges with Ultra Long Spans. 1988.
R 241. NIELSEN, LEIF OTTO: En Reissner–Mindlin Plade Element Familie. 1989.
R 242. KRENK, STEEN og THORUP, ERIK: Stochastic and Concrete Amplitude Fatigue Test of Plate Specimens with a Central Hole. 1989.
R 243. AARKROG, P., THORUP, E., KRENK, S., AGERSKOV, H. and BJØRNBAK–HANSEN, J.: Apparatur til Udmattelsesforsøg. 1989.
R 244. DITLEVSEN, OVE and KRENK, STEEN: Research Workshop on Stochastic Mechanics, September 13–14, 1988.
R 245. ROBERTS, J.B.: Averaging Methods in Random Vibration. 1989.
R 246. Resumeoversigt 1988 – Summaries of Papers 1988. 1989.
R 247. GIMSING, N.J., JAMES D. LOCKWOOD, JAEHO SONG: Analysis of Erection Procedures for Cable–Stayed Bridges. 1989.
R 248. DITLEVSEN, O. og MADSEN, H.O.: Proposal for a Code for the Direct Use of Reliability Methods in Structural Design. 1989.
R 249. NIELSEN, LEIF OTTO: Simplex Elementet. 1989.
R 250. THOMSEN, BENTE DAHL: Undersøgelse af "shear lag" i det elasto–plastiske stadium. 1990.
R 251. FEDDERSEN, BENT: Jernbetonbjælkers bæreevne. 1990.
R 252. FEDDERSEN, BENT: Jernbetonbjælkers bæreevne, Appendix. 1990.
R 253. AARKROG, PETER: A Computer Program for Servo Controlled Fatigue Testing Documentation and User Guide. 1990.
R 254. HOLKMANN OLSEN, DAVID & NIELSEN, M.P.: Ny Teori til Bestemmelse af Revneafstande og Revnevidder i Betonkonstruktioner. 1990.
R 255. YAMADA, KENTARO & AGERSKOV, HENNING: Fatigue Life Prediction of Welded Joints Using Fracture Mechanics. 1990.
R 256. Resumeoversigt 1989 – Summaries of Papers 1989. 1990.
R 257. HOLKMANN OLSEN, DAVID, GANWEI, CHEN, NIELSEN, M.P.: Plastic Shear Solutions of Prestressed Hollow Core Concrete Slabs. 1990.
R 258. GANWEI, CHEN & NIELSEN, M.P.: Shear Strength of Beams of High Strength Concrete. 1990.
R 259. GANWEI, CHEN, NIELSEN, M.P. NIELSEN, JANOS, K.: Ultimate Load Carrying Capacity of Unbonded Prestressed Reinforced Concrete Beams. 1990.
R 260. GANWEI, CHEN, NIELSEN, M.P.: A Short Note on Plastic Shear Solutions of Reinforced Concrete Columbs. 1990.
R 261. GLUVER, HENRIK: One Step Markov Model for Extremes of Gaussian Processes. 1990.

Abonnement 1.7.1990 – 30.6.1991 kr. 130,–
Subscription rate 1.7.1990 – 30.6.1991 D.Kr. 130.–.

Hvis De ikke allerede modtager Afdelingens resumeoversigt ved udgivelsen, kan Afdelingen tilbyde at tilsende næste års resumeoversigt, når den udgives, dersom De udfylder og returnerer nedenstående kupon.

Returneres til
Afdelingen for Bærende Konstruktioner
Danmarks tekniske Højskole
Bygning 118
2800 Lyngby

Fremtidig tilsendelse af resumeoversigter udbedes af
(bedes udfyldt med blokbogstaver):

Stilling og navn: .....

Adresse: .....

Postnr. og -distrikt: .....

The Department has pleasure in offering to send you a next year's list of summaries, free of charge. If you do not already receive it upon publication, kindly complete and return the coupon below.

To be returned to:
Department of Structural Engineering
Technical University of Denmark
Building 118
DK-2800 Lyngby, Denmark.

The undersigned wishes to receive the Department's
List of Summaries:
(Please complete in block letters)

Title and name .....

Address.....

Postal No. and district.....

Country.....